USGS
science for a changing world

Prepared for the National Aeronautics and Space Administration

Geologic Map of the Helen Planitia Quadrangle (V–52), Venus

By Iván López and Vicki L. Hansen

Pamphlet to accompany
Scientific Investigations Map 3026

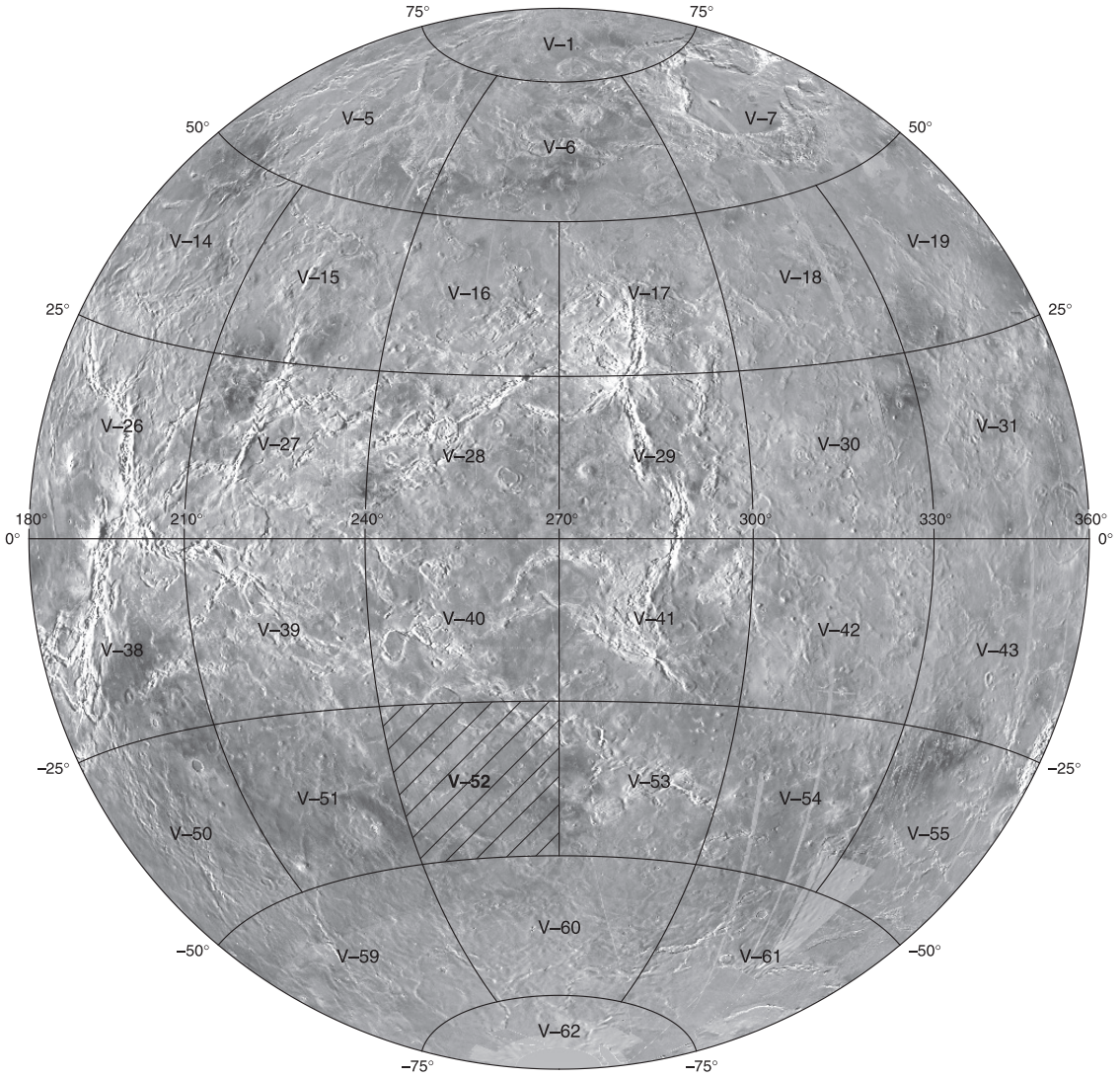

2008

U.S. Department of the Interior
U.S. Geological Survey

Contents

The Magellan Mission

The Magellan spacecraft orbited Venus from August 10, 1990, until it plunged into the Venusian atmosphere on October 12, 1994. Magellan Mission objectives included (1) improving the knowledge of the geological processes, surface properties, and geologic history of Venus by analysis of surface radar characteristics, topography, and morphology and (2) improving the knowledge of the geophysics of Venus by analysis of Venusian gravity.

The Magellan spacecraft carried a 12.6-cm radar system to map the surface of Venus. The transmitter and receiver systems were used to collect three data sets: (1) synthetic aperture radar (SAR) images of the surface, (2) passive microwave thermal emission observations, and (3) measurements of the backscattered power at small angles of incidence, which were processed to yield altimetric data. Radar imaging and altimetric and radiometric mapping of the Venusian surface were accomplished in mission cycles 1, 2, and 3 from September 1990 until September 1992. Ninety-eight percent of the surface was mapped with radar resolution on the order of 120 m. The SAR observations were projected to a 75-m nominal horizontal resolution, and these full-resolution data compose the image base used in geologic mapping. The primary polarization mode was horizontal-transmit, horizontal-receive (HH), but additional data for selected areas were collected for the vertical polarization sense. Incidence angles varied between about 20° and 45°.

High-resolution Doppler tracking of the spacecraft took place from September 1992 through October 1994 (mission cycles 4, 5, 6). Approximately 950 orbits of high-resolution gravity observations were obtained between September 1992 and May 1993 while Magellan was in an elliptical orbit with a periapsis near 175 km and an apoapsis near 8,000 km. An additional 1,500 orbits were obtained following orbit-circularization in mid-1993. These data exist as a 75° by 75° harmonic field.

Magellan Radar Data

Radar backscatter power is determined by (1) the morphology of the surface at a broad range of scales and (2) the intrinsic reflectivity, or dielectric constant, of the material. Topography at scales of several meters and larger can produce quasi-specular echoes, and the strength of the return is greatest when the local surface is perpendicular to the incident beam. This type of scattering is most important at very small angles of incidence, because natural surfaces generally have few large tilted facets at high angles. The exception is in areas of steep slopes, such as ridges or rift zones, where favorably tilted terrain can produce very bright signatures in the radar image. For most other areas, diffuse echoes from roughness at scales comparable to the radar wavelength are responsible for variations in the SAR return. In either case, the echo strength is also modulated by the reflectivity of the surface material. The density of the upper few wavelengths of the surface can have a significant effect. Low-density layers, such as crater ejecta or volcanic ash, can absorb the incident energy and produce a lower observed echo. On Venus, a rapid increase in reflectivity exists at a certain critical elevation above which high-dielectric minerals or coatings are thought to be present. This leads to very bright SAR echoes from virtually all areas above that critical elevation.

The measurements of passive thermal emission from Venus, though of much lower spatial resolution than the SAR data, are more sensitive to changes in the dielectric constant of the surface than to roughness. They can be used to augment studies of the surface and to discriminate between roughness and reflectivity effects. Observations of the near-nadir backscatter power, collected using a separate smaller antenna on the spacecraft, were modeled using the Hagfors expression for echoes from gently undulating surfaces to yield estimates of planetary radius, Fresnel reflectivity, and root-mean-square (rms) slope. The topographic data produced by this technique have horizontal footprint sizes of about 10 km near periapsis and a vertical resolution on the order of 100 m. The Fresnel reflectivity data provide a comparison to the emissivity maps, and the rms slope parameter is an indicator of the surface tilts, which contribute to the quasi-specular scattering component.

Helen Planitia Quadrangle

Introduction

The Helen Planitia quadrangle (V–52), located in the southern hemisphere of Venus between lat 25° S. and 50° S. and between long 240° E. and 270° E. (fig. 1*A*), covers approximately 8,000,000 km^2 (fig 1, map sheet). Regionally, the map area is located at the southern limit of an area of enhanced tectonomagmatic activity and extensional deformation, marked by a triangle that has highland apexes at Beta, Atla, and Themis Regiones (BAT anomaly) and is connected by the large extensional belts of Devana, Hecate, and Parga Chasmata (Crumpler and others, 1993). The BAT anomaly covers approximately 20 percent of the Venusian surface (Crumpler and others, 1997).

Helen Planitia quadrangle (V–52), bounded to the east by Themis Regio, a corona-dominated rise, and to the west by Wawalag Planitia, represents an area of topographic transition between the highlands of Phoebe and Themis Regiones and the lowlands of Helen Planitia. Within the map area, another topographic transition occurs between the mesoland of eastern Parga Chasmata that dominates the north and the lowland of northern Helen Planitia in the south (fig. 1*B*, map sheet). Parga Chasmata, a northwest-trending 10,000-km-long fracture and trough system, connects Atla and Themis Regiones (for example, Stofan and others, 1992; Stofan and others, 1997). The Parga Chasmata system consists of 14 branching segments; two occur in the map area, associated with coronae and other tectonomagmatic structures. The southern map area hosts the volcanic plains of northern Helen Planitia, where the most prominent topographic features describe a network of broad warps and elevated areas that form the boundary with the rest of the map area (fig. 2*A*, map sheet). The central map area marks the transition between these two different geologic and topographic regions.

The location between the Parga Chasmata mesoland and the Helen Planitia lowland and the high concentration of features indicative of extensional tectonic processes and volcanic activity make Helen Planitia quadrangle an excellent region to test differing, and debated, models of Venus geological evolution (Basilevsky and others, 1997; Phillips and Hansen, 1998; Guest and Stofan, 1999).

Data and Methodology

The U.S. Geological Survey digital FMAP SAR imagery (75 m/pixel) and derived products form the map base. Adobe Illustrator™ 8, 9, and 10 were the primary mapping tools; image processing was accomplished using Adobe Photoshop™ 5. Ancillary data included Global Topographic Data Record 3 (GTDR 3), as well as Fresnel reflectivity at wavelengths of 12.8 cm, average meter-scale slope, and derived 12.8 cm emissivity data (GRDR, GSDR, and GEDR, respectively; figs. 2*B*, 2*C* and 2D, map sheet). GTDR data were combined with SAR images to produce synthetic stereo anaglyphs (Kirk and others, 1992) using NIH-Image macros developed by D.A. Young (University of Minnesota Duluth). These images played a critical role in elucidating relations between geology and topography and, in particular, interaction of flows, primary and secondary structures, and topography.

The interpretation of features in Magellan S-band SAR imagery is key to developing a geologic history for the Helen Planitia quadrangle (V–52). The subject of radar image interpretation is explored in depth in Ford and others (1993).

Kilometer-scale slopes are resolved in radar images as systematic variations in radar backscatter; radar-facing slopes scatter more radiation than slopes facing away from radar. Converting the range data that SAR provides into a plan-view projection introduces geometric distortions that provide topographic information. Because SAR is sensitive to slight variations in slope along the spacecraft look direction, topography is highlighted, though difficult to constraint quantitatively.

SAR data is also sensitive to surface roughness at the scale of radar wavelength (12.8 cm); rough surfaces appear bright and smooth surfaces appear dark. These variations are textural, and a direct correlation with material type cannot be assumed. Variation in pahoehoe to aa surfaces within individual terrestrial lava flows presents an analogous problem.

A key assumption in the interpretation of the Venus rock record is that liquid water has not played a role in shaping the surface. Primary evidence for this assumption is rooted in the extremely dehydrated state of the lower atmosphere (Donahue and others, 1997) and lithosphere (Mackwell and others, 1998) and the present surface temperature of approximately 460°C (Crisp and Titov, 1997). The lack of surface water and its erosional processes argues against widespread occurrence of exposure of deep crustal metamorphic rocks (no erosion) or sedimentary rocks (no deposition). Exceptions relate to impact craters. Impact crater rim material presumably underwent shock metamorphism, and fine ejecta was presumably redistributed and deposited by wind, comprising limited aeolian sedimentary facies (Greeley and others, 1992). Bulk chemical analyses of the surface resulting from the Venera Mission may represent subsurface material excavated by impact craters and redistributed across the surface, providing subsurface compositional data (Basilevsky and Head, 2004). Although deep crustal metamorphic facies might not be typically exposed on the Venusian surface, current surface conditions lie within the metamorphic hornfels facies (~475°C, 92 bars). Furthermore, surface temperature could have been higher in the past (Bullock and Grinspoon, 2001; Phillips and others, 2001). Thus, material exposed at the surface is metamorphic by terrestrial standards, although metamorphism presumably occurred in situ.

Geologic map construction is a critical first step in unraveling geologic history, which provides critical relations for understanding the range of processes that contributed to planet evolution. Because geologic mapping is an interpretation that results in a database to be used for further interpretation of geological processes (Butler and Bell, 1988; Maltman, 1990), mapping methodology must not predetermine the geologic map. Secondary structures (strain) should be clearly differentiated from geologic units (materials), because materials and structures record different time slices in a surface evolution and they also reflect different aspects of past processes. Our methodology for the definition of geological units and structural fabrics builds on standard geological analysis detailed in Wilhelms (1990) and Tanaka and others (1994), with cautions of Hansen (2000), Zimbelman (2001), Skinner and Tanaka (2003), and McGill and Campbell (2004). Map units represent material emplaced within an increment of geological history, to which standard stratigraphic methods have some limited application. However, some units are most likely composite; they might not be stratigraphically coherent over their entire represented area, and (or) they may have been emplaced time transgressively in relation to other units and (or) the formation of secondary structures. To further complicate both temporal constraints and history, evidence for reactivation of secondary structures is common.

The term “terrain” is used to describe a texturally defined region. Characteristic texture could imply a shared history, similar to terrestrial gneissic terrain that is used to describe a particular shared history, such as a tectonothermal event responsible for melding possibly previously unrelated rock units (any combination of igneous, metamorphic, and sedimentary rocks) into a new package. As with gneissic terrain, we do not mean to infer any unique history prior to the event(s) that melded potentially separate units into a composite textural terrain. Events prior to terrain formation would be unconstrained unless specifically noted.

Criteria for distinguishing discrete geological (as opposed to radar) units include the presence of sharp, continuous contacts; truncation of, or interaction with, secondary structures and topography; and primary structures (for example, flow channels or edifice topography) that allow a reasonable geological interpretation and hint at a three dimensional geometry. Some mapped units fail to fit these constraints, limiting their use in constructing stratigraphic sequences. Composite units, in particular, cannot provide robust temporal constraints, even of a relative nature.

Both primary (depositional) and secondary (tectonic) structures are identified in the Magellan SAR data. Primary

structures include channels, shields, lobate flow fronts, and impact crater haloes and rims. Channels represent sinuous low-backscatter features hundreds of kilometers long and a few kilometers wide; locally they lack apparent topographic relief (Baker and others, 1992). Because Venus is dry, low-viscosity lava is perhaps the most likely fluid to form these features. Shields are small (diameter generally 2–15 km, rarely 20 km), quasi-circular to circular, low- to high-backscatter features with or without topographic expression and with or without a central pit. The size of individual shields can be difficult to constrain because their bases are commonly poorly defined, and deposits can blend smoothly into a layer of coalesced deposits. Shields likely represent the manifestation of local volcanic flows (Guest and others, 1992; Crumpler and others, 1997; Addington, 2001). Shields and associated deposits form a composite unit that cannot be robustly treated as a timeline or marker unit (Hansen, 2005). Pits, sharply defined depressions, or pit chains, which are linear arrays of pits, likely represent regions marked by subsurface excavation; they may mark the surface expression of dilatational faults or dikes (Okubo and Martel, 1998; Bleamaster and Hansen, 2001; Ferrill and others, 2004; Schultz and others, 2004).

Most radar lineaments represent secondary structures. Extremely fine, sharply defined, continuous, radar-bright lineaments, typically occurring in the lowland, are interpreted as fractures (for example, Banerdt and Sammis, 1992; Banerdt and others, 1997; DeShon and others, 2000). If the fracture is associated with pits, the fracture probably represents the surface expression of a subsurface dike or a dilational fault. Paired dark and light lineaments that describe linear troughs more than a few kilometers across are interpreted as graben.

In SAR imagery, the opposite of a groove (linear trough) is a ridge (positive linear topography marked by light and dark lineaments a few kilometers across with the light lineament closest to illumination direction). On Venus, ridges either have parallel edges with moderate sinuosity at the 10-km scale and have an across-strike gradation in backscatter (a form we specifically call ridges) or they have a more erratic plan view that contains frequent right-angle interruptions at the 10-km scale and variations in across-strike width (wrinkle ridges). Positive linear topographic features, hundreds of kilometers across and as much as thousands of kilometers long, are too subtle to appear prominently in SAR data, but they are visible in topographic data and are called warps.

Parallel bright and dark lineaments that defined alternating parallel ridges and troughs and have typical wavelengths of 2–5 km are called ribbon fabric (Hansen and Willis, 1998). Ribbon fabrics are commonly associated with fold structures that trend at a high angle to the ribbon lineaments and with graben that commonly parallel ribbon trends but can be differentiated from the ribbons on the basis of smaller length:width ratios. Collectively referred to as ribbon terrain, this distinctive tectonic fabric commonly marks tessera terrain. The composite fabric may reflect a progressive increase in the depth to the rheological brittle-ductile transition (BDT) with time and fabric development (Hansen and Willis, 1998; Hansen and others 1999; Hansen, 2006). For an alternative view of ribbon-terrain formation see Gilmore and others (1998).

Interpretation of geologic structures, material units, temporal relations among the structures and material units, and ultimately the geologic history using Magellan SAR data requires the same careful consideration that should be employed with any remote sensing data set (Wilhelms, 1990; Tanaka and others, 1994; Hansen, 2000). Radar data permit mapping of surface morphologies and structures (Daily and Stewart, 1979; Ford and others, 1989, 1993). Geologic unit boundaries can be defined by radar backscatter intensity and (or) by crosscutting relations among materials or by topographic features. Gradational contacts can be difficult to trace. The termination of tectonic structures could represent the spatial limit of a deformation front or the limit of younger onlapping material; whereas, structural facies boundaries typically represent a strain discontinuity related to a tectonic process (perhaps marked by a decrease in structural element density). Young burial is more likely if the truncation of structural elements occurs at a high angle to the structural trend. These determinations can help establish local sequences of events, but they are not applied to a composite unit. The degree of uncertainty of stratigraphic position is noted in unit descriptions.

Another problem in establishing regional sequences results from the absence of reliable time markers or marker units. Any marker unit must (1) be unique, (2) have formed quickly, and (3) cover a large region (Compton, 1985, p. 85). Terrestrial examples of a marker unit include air-fall tuff, sedimentary layers marked by unique fossils or mineral assemblages, or geomagnetic polarity. Terrestrial studies also typically include radiometric ages that constrain absolute time and enhance confidence in unit correlations. None of these methods are available for Venus. Correlation of map units in planetary maps is typically based on surface impact-crater statistics. Although this method has some utility for planetary bodies with old surfaces and high crater densities (for example, Moon and Mars), many problems arise on Venus because of crater-population characteristics. Fundamentally, Venus impact craters cannot place constraints on the age of surface units that cover the small areas within the Helen Planitia quadrangle (Hauck and others, 1998; Campbell, 1999).

As a result of these limitations, we establish local geological histories following geologic and geographic criteria, where units are in contact and (or) interact with the different structural suites. We define two regions in the map area (Parga Chasmata region and Helen Planitia region, fig. 1*B*) that are each separated into three sectors: western, central, and eastern. In these regions and subregions, we confidently define local temporal relations between the different units. These temporal constraints are only locally applicable and cannot be robustly extended across the map area, much less to adjacent regions. Geologic mapping is ultimately built on consistency arguments; observations, assumptions, and interpretations should always be open to question (Gilbert, 1886). Unfortunately, at this point in Venus geologic investigation, there is no robust means available to correlate regional surface units without operative assumptions that would deem any correlation circular. If we did not divide the map area into subregions, we believe no robust unit correlations could be made. Thus, the division of the map area into subregions allows us to propose limited unit correlation. Temporal

relations between some units can be established in more than one of these regions and subregions, especially in the areas of contact/transition between them, although the unit is described in the area where the unit type locality is defined. Widespread materials that form undivided units are located across the map area.

Map Units

The topography and geology of the Helen Planitia quadrangle (V–52) is divisible into two major regions, the Parga Chasmata region (PCR) in the north and the Helen Planitia lowland/region (HPR) in the south. The extensional belt of Parga Chasmata dominates the northern map area and influences the type and distribution of the geologic materials and the trend and style of deformation. Many large tectonomagmatic features and their associated materials are geographically linked with Parga Chasmata. The southern map area displays different deformation trends and a multitude of large tectonomagmatic features, whose distribution and related materials differ from those of the chasmata. Widespread materials (undivided units) that occur throughout the map area are described separately.

Widespread Materials

Tessera terrain, undivided (unit tu) is exposed in a group of inliers and small outcrops distributed across the map area and contains intersecting suites of tectonic lineaments, high surface roughness, and positive relief relative to surrounding deposits. Individual inliers display different structural assemblages and deformational histories, and the relative timing among and between inliers is unconstrained.

In the western PCR (lat 26.0° S., long 241° E.), unit tu displays northeast-trending, ribbon-like structures. Although the ribbon structures are highly degraded and locally embayed by surrounding volcanic material, the constant width, spacing, and high length:width ratio that characterizes ribbon fabric (Hansen and Willis, 1998) is preserved. A suite of troughs (interpreted as graben) and northwest-trending fractures cut the ribbon fabric and the surrounding materials. East-northeast-trending lineaments may represent fold crests, but their near-parallel orientation relative to radar illumination inhibits robust geometric characterization. The relative timing of ribbon fabric and the east-northeast lineaments is unconstrained. Unit tu in the western PCR also includes several small kipukas of extremely deformed material. Deformation fabrics mask the character of the predeformational terrain and even inhibit clear identification of the character of the tectonic structures. Individual linear structures are about 1 km wide and are arranged in subparallel sets that generally trend northwest, although some structures in isolated outcrops trend north-northwest. Similar materials have been named densely lineated plains material (for example unit pdf, Ivanov and Head, 2001); these workers state that their coresponding unit always occurs stratigraphically above tessera terrain (for example, Basilevsky and Head, 1995), and they assume that the precursor material was volcanic plains material composed of mafic lavas (Basilevsky and Head, 2000). Because penetrative deformation, or deformation fabric marked by very closely spaced lineaments relative to the scale of observation, precludes observation of precursory material and stratigraphic relations can only be locally extrapolated, we are not comfortable extending these previous assumptions to units in the map area.

A group of inliers of unit tu geographically related to Giltine Tesserae dominates the central and western part of the PCR. Some inliers display small isolated shields emplaced after tessera terrain deformation and are likely unrelated to the original formation of the unit materials. The degree of preservation of the different structures due to embayment by younger material varies among inliers. Crosscutting structures show evidence of tectonic reactivation and topographic modification, making the interpretation of some of the original characteristics of unit tu difficult. The inlier located at lat 39° S., long 248.5° E. preserves the best example of ribbon-like structures in the map area. These ribbon troughs, classified as tensile-fracture ribbons (Hansen and Willis, 1998), display a consistent northwest trend, an approximately 2 km width, and a regular spacing of approximately 2.5 km. Northeast-trending graben cut ribbons as illustrated in several inliers of unit tu; the graben are embayed by younger volcanic materials. Other tessera-terrain inliers display structures that could also be ribbons, but modification by later local tectonic structures or volcanic embayment frustrates efforts to quantitatively characterize these structures.

In the western HPR, unit tu comprises several large inliers and many small kipukas that crop out in Sopdet Tesserae, Tsovinar Dorsa, and Kastiatsi Dorsa and within Hlineu Corona—elevated areas that define long northwest- and northeast-trending topographic arches bordering Helen Planitia. In these locations, unit tu displays different suites of secondary structures that mostly trend parallel to the northwest trend of the inliers: closed-spaced ridge and fracture tectonic fabric and folds located preferentially along the margins of the large inliers. Another penetratively developed, subtle, northeast-trending lineament suite cuts some inliers (for example, lat 44.5° S., long 251.5° E.); SAR image resolution does not allow structural characterization. Late arcuate and north-northeast-trending graben cut northwest-trending ridge and fracture fabrics; graben are embayed by younger volcanic materials that surround unit tu.

In the central and eastern parts of HPR, along the border with the Godiva quadrangle (V–60), unit tu forms a group of large inliers and small kipukas named Norna Tesserae. Intratessera volcanic material occurs within unit tu in basins in the southernmost inlier. The inliers that form unit tu show differences in their deformation fabrics. In the southernmost limit of eastern HPR, an inlier located at lat 50° S., long 263° E. displays orthogonal suites of secondary structures: northeast-trending, fine-scale lineaments; northwest-trending, ribbon-like fabric with troughs spaced <2 km; northwest-trending, graben-like structures; and northeast-trending folds that have a wavelength of about 10 km. Temporal relations between ribbons and folds is unconstrained due to image resolution, although the longer wavelength of the folds relative to ribbons is consistent with younger fold formation (Hansen and Willis,

1998; Ghent and Hansen, 1999; Brown and Grimm, 1997). A north-northeast-trending late graben that has a width of ~15 km postdates ribbons and folds. The inliers located at lat 48.5° S., long 264.5° E. and lat 47.5° S., long 268° E. also display high radar backscatter and a blocky texture; the predominant deformation fabric is composed of a suite of northwest-trending fractures and ridges that lack the periodicity of the ribbon fabric. In some small kipukas, two intersecting sets of northwest- and northeast-trending orthogonal graben postdate the northwest-striking structures. Late flows and shield-related materials embay the graben. The inlier located at lat 48.5° S., long 264.5° E. is cut by Sinnan Vallis. Other outcrops of unit tu located around and in Enekeler Corona display a fine-scale, north-northwest-trending, tectonic fabric below image resolution. Small outcrops located in Enekeler Corona display east-trending graben that postdate the north-northwest-trending lineaments.

In eastern HPR a large inlier and a group of small kipukas of unit tu form Ustrecha Tessera. In local sections of the inlier, north-trending lineaments form a penetrative fabric with an indeterminate morphology and origin. A radial fracture suite also cuts this inlier, but temporal relations between the north-trending structures and the radial fracture suite are unclear due to embayment relations and possible structure reactivation. It is unknown if the radial fracture set is related to emplacement of unit tu or if it comprises a local fracture set that overprints unit tu. A set of east-northeast-trending graben postdate structures of unit tu and the surrounding fractures. Many shields and associated materials occur in spatial association with unit tu, but these primary structures are interpreted to postdate unit tu formation.

Heterogeneous material, undivided (unit hu), is composed of undifferentiated materials distributed across the map area. Unit hu represents a composite unit without stratigraphic significance that combines materials of different origin, and probable different age, that cannot be confidently differentiated with available data. We use the unit name, heterogeneous materials, undivided, because unit hu includes a range of volcanic styles, including different corona-, volcano-, and shield-related materials of low to intermediate-high backscatter and homogeneous to mottled texture. Many volcanic and large tectonomagmatic features are located on unit hu. Large flow units are difficult to delimit, perhaps due to radar homogenization of flows with time (Arvidson and others, 1992). Primary structures are, however, identified in unit hu, providing evidence of the multiple genetic processes and distinct source locations implied in material emplacement. Individual lobate fronts are mapped in unit hu; some flows can be traced to a definite source, such as Chuginadak Mons and Darclée Patera, but the origin of others is uncertain. Helen Planitia contains a high concentration of channels (Baker and others, 1997); most channels in the map area occur in unit hu. One channel, Sinnan Vallis, extends for 450 km eastward from southeastern V–52 into V–53. Other channels, some partially buried, show no recognized source, supporting the composite nature of unit hu. In addition, hundreds to thousands of small shields are scattered across unit hu. The point-sourced character of shield deposits makes it difficult to establish shield-related map units (Guest and others, 1992; Hansen, 2005). SAR relations indicate multiple individual shields instead of accumulations associated with individual flows. Shields and shield clusters are especially numerous in southern and southeastern Helen Planitia. Many of the shield fields in unit hu are spatially associated with large tectonomagmatic features such as coronae (Tangba Corona). Other isolated shields and shield-related material are related to the regional fractures that both postdate shields and are overprinted by shields, indicating time transgressive processes. Unit hu also displays medium-size volcanoes and steep-sided domes, but no distinct flow materials are mapped in relation to these volcanic features. The relation of unit hu with the surrounding material is difficult to establish due to the composite and undifferentiated nature of unit hu. Unit hu locally postdates local tessera terrain (unit tu). Unit hu appears to correlate with Chapman's flow material (1999, unit f_2), which underlies corona-related materials. Unit hu also appears to correlate with the regional plains material of Johnson and others (1999, unit pr, V–59). The character and regional significance of each of these composite units is defined and interpreted within the context of their local geologic settings, and direct correlation between these units is not assumed. Unit hu does not correlate with unit plains with wrinkle ridges of Basilevsky and Head (1998, 2000, units pwr_1 or pwr_2), because unit hu shows a wide range of contributing sources and was emplaced time-transgressively.

Different impact structures and associated materials are distributed across the map area (both PCR and HPR). Impact-related primary structures (rim and central peak) are mapped as primary structures for each crater; whereas, crater-ejecta material and crater-floor material are mapped as crater material (unit c). Because each impact crater formed individually in space and time, we only consider the stratigraphic position of individual impact craters. Implications for material ages are not statistically robust (Campbell, 1999) and, therefore, are not considered.

Two craters, Rose and Wollstonecraft, show extensive distal outflow deposits mapped as crater flow material (unit cf). Rose displays a north-flowing, radar-rough, outflow material that locally interacts with preexisting northeast-trending fractures that channeled the flow. Schultz (1992) classified this crater as result of an oblique impact from the south. Apart from the direction of the outflows, Schultz (1992) used the blast pattern on the surrounding structures and established a change from turbulent flow near the crater to laminar and channeled flow through the fractures to the north. The other crater with an associated outflow, Wollstonecraft, displays butterfly-wing ejecta morphology, proposed as indicative of a low-impact angle (Schultz, 1992). The slightly elongated shape of the crater along an east-trending axis is also consistent with oblique impact. The west-flowing, extensive outflow of Wollstonecraft, which postdates unit hu, is formed by an intermediate-backscatter flow with a radar-rough inner section. The outflow displays bright edges along its perimeter, which indicates a rougher texture. The outflow covers portions of the radial fracture system (lat 40.5° S., long 258° E.), although the fractures are locally visible through the outflow; these relations indicate that the outflow forms a thin layer. The outflow is also locally ponded along north-trending wrinkle ridges.

Sequence of Materials in the Parga Chasmata Region

The Parga Chasmata region (PCR) hosts several major units including Parga Chasmata materials, corona-related flows, shield-dominated units, and local volcano-related flows and heterogeneous materials (see Widespread Materials). Structurally, the PCR is dominated by the regional-scale, northwest-trending Parga Chasmata and numerous radial and concentric local structural suites associated with coronae emplaced within and near Parga Chasmata. Flows are locally cut by coronae and chasmata-related fractures; yet these flows also locally overprint the fractures, suggesting that tectonic and volcanic activity overlapped in space and time and may be genetically related. Each unit is discussed by temporal formation from old to young, development from more extensive to more localized, and location spatially from east to west. We end the discussion with two units that display gradational characteristics with adjacent units.

Parga Chasmata materials a, b, and c (units Pa, Pb, Pc) are basal units commonly associated with local highs (although not all basal units correlate with local highs and not all local highs correlate with the exposure of these basal units). These basal materials also underlie the corona- and volcano-related materials in the PCR. Emplacement mechanisms for the Parga Chasmata materials are not well constrained, but the presence of small shields and the flow-like, embayment relations with older materials suggest that polygenetic volcanic processes may have been important. We separate these three units in terms of backscatter, topography, and tectonic fabric, a practice that should be avoided if possible (Hansen, 2000). In this case, the different geographic locations, radar characteristics, and presence of primary structures and the different character and wavelength of the deformational structures allow us to divide Parga Chasmata materials into these three units; note, however, we have no evidence for temporal relations among the units.

Parga Chasmata material a (unit Pa) displays homogeneous texture and intermediate to high backscatter due to crosscutting fractures. In western PCR, unit Pa lies topographically above the surrounding materials that embay it (unit hu and corona-related materials that dominate the PCR), although this relation is locally unclear due to gradual topographic transitions with surrounding materials. Unit Pa hosts numerous individual shields that locally cluster (for example, lat 25.5° S., long 242° E.). Unit Pa is cut by multiple sets of local fractures of various orientations; the fractures do not cut the surrounding materials and, thus, predated emplacement of those materials. Part of unit Pa (lat 26° S., long 241.5° E.) is cut by a set of regional, northwest-striking fractures that extend into the surrounding units. Locally the fractures do not extend far into adjacent units; this may be due to subsequent emplacement of local cover material. Unit Pa embays the structural topography of unit tu and postdates deformation associated with the formation of unit tu at this location.

In the central PCR, unit Pa forms one large outcrop and three small kipukas. Most of unit Pa lies within a topographic high related to Parga Chasmata. Topographically, the contact of unit Pa with the surrounding materials is gradational and occurs within this elevated area. Closely spaced fractures and graben are penetratively developed across unit Pa and prevent characterization of the original material. The main fracture trends that affect unit Pa are (1) north-striking fractures and (2) regional northwest-trending fractures and graben that form a small branch of Parga Chasmata and postdate the north-striking fractures. In addition, a local suite of concentric fractures cuts unit Pa. Although the concentric fractures could be related to a local tectonomagmatic structure, for example, caldera or small corona, evidence of associated flow material is lacking.

Parga Chasmata material b (unit Pb) is composed of topographically elevated materials of high backscatter. Unit Pb displays a tectonic fabric composed of fractures and troughs, including some ribbon-like structures; but embayment by younger flows inhibits classification. The outcrop centered at lat 30.5° S., long 268° E. shows a deformation fabric comprised of fractures and graben of Parga Chasmata and local radial structures of tectonomagmatic origin, such as coronae and novae. Younger material locally covers these fractures, yet the material is subsequently deformed along reactivated fractures. Material similar to unit Pb occurs in the Galindo quadrangle (V–40; Chapman, 1999), located north of the map area. Chapman (1999) maps this terrain following two different interpretations: tessera terrain (Tessera materials of Phoebe Regio, unit tpr) or volcano-related material (Mons materials unit a, unit m_a).

Parga Chasmata material c (unit Pc) is a composite unit of volcanic origin located in the eastern limit of the PCR. Unit Pc, marked by heterogeneous texture and an intermediate backscatter signature, displays many volcanic structures and large tectonomagmatic features with associated flows. Clusters of shields and many isolated shields occur within unit Pc. It is not clear if the shields were emplaced during or after the emplacement of the materials that form unit Pc. A fine-scale reticulate tectonic fabric occurs in the southern boundary and center of unit Pc. The reticulate pattern is composed of two intersecting fracture trends, north-northwest and west-northwest, both formed by single lineaments with a constant interfracture spacing <2 km and lengths over 100 km. Another intersecting set of north-northeast- and northwest-trending fractures and graben cut unit Pc along its western boundary. These fracture suites do not cut the overlying materials and, therefore, provide temporal constraints among unit Pc, formation of the fractures, and emplacement of younger surrounding units. Local, ridge-like, northeast-trending lineaments with a regular spacing <2 km deform unit Pc. Although these structures appear to postdate the fractures, temporal relations cannot be robustly established.

Five corona-related units, four volcano-related, and four units formed by shields and shield-related materials overly the tessera terrain and Parga Chasmata materials.

Shield field and associated materials near Nordenflycht Patera (unit sfN,) are emplaced over basal unit Pc in an unnamed circular tectonomagmatic feature south of Nordenflycht Patera. Unit sfN, formed by low-backscatter and homogeneous-texture material, displays shields that may be the unit source. Unit sfN locally buries and, therefore, postdates northeast-trending fractures in the interior of the tectonomagmatic structure.

Flow material from Otohime Tholus (unit ftO,) is composed of intermediate backscatter flows arranged around Otohime Tholus. Otohime Tholus displays steep scarps but no associated debris apron, which is probably covered by some of the flows. Close-spaced, north-northwest-striking fractures deform unit materials, yet these fractures are also partly covered by flows to the east of the tholus. Flows of unit ftO postdate unit Pc but are, in turn, partly covered by younger fracture- and corona-related flows and individual shields.

Flow material from Mertseger Mons (unit fmM;) is composed of multiple overlapping flows of low to intermediate backscatter arranged radial to Mertseger Mons, an approximately 2-km-high, nova-like structure located on the east border with the Themis Regio quadrangle (V–53). The lobate, finger-like morphology and the presence of flows that have leveed channels help to constrain the direction, maximum extent, and emplacement mechanisms of unit fmM flows. There is a transition from low-backscatter materials in the distal portion of unit fmM to intermediate-backscatter flows that present bright edges on the sides oriented toward the left-looking radar antenna; this radar facies may reflect volcanic flow facies related to unit emplacement. Unit fmM also hosts many individual, small shields, which are grouped near the summit of Mertseger Mons. In the summit region, a suite of radial fractures and graben occur with the extensive flow field at their termination. Some radial fractures display pits—evidence of dilational faults and (or) dikes and subsurface magma transport. Contacts with basement materials of unit Pc are clear; distal flows of unit fmM postdate fine-scale deformation patterns that characterize the local basal unit. Flows of unit fmM locally overlap and, therefore, postdate materials of unit hu, but this relation cannot be regionally extrapolated.

Flows and shield-related materials around Zerine crater (unit fsZ;) embay unit Pa in northern Helen Planitia quadrangle (V–52). Unit fsZ shows variable backscatter with intermediate to high values and forms a composite unit comprising corona-related flows, shields and shield-related flows, and materials of no assignable origin located in the vicinity of Zerine. Unit fsZ displays flows of lobate morphology and high-backscatter flows disposed in different directions around an unnamed corona (lat 28.5° S., long 258° E.). Shields within the unit cluster in two distinct areas, each with different characteristics. The first shield field (lat 28.5° S., long 256.5° E.) includes multiple <10-km-diameter edifices with associated high backscatter material and postdates a local, subtle, northeast-trending fracture system and the local, radial, fracture suite associated with the unnamed corona that is the source of the flows. Graben of Parga Chasmata are postdated by this shield-related material; some shields are aligned with the northwest trend of the structures of Parga Chasmata, suggesting that these fractures and graben locally control shield emplacement. A steep-sided dome occurs close to the shield field; it postdated both the materials of unit fsZ and the regional fractures, likely representing a late volcanic episode of unit fsZ. The second shield field (lat 29° S., long 254° E.) includes shields that display channels and associated flows; some shields have pits elongated in the direction of preexisting northwest-striking fractures, suggesting structural control of shield emplacement. Temporal relations between the two described shield fields are unconstrained.

Corona-related flows dominate the PCR. Most of the coronae, where these flows originate, lie along Parga Chasmata, although some off-rift features that contain important volcanic flows are also present (for example, Oanuava Corona). Flow material from fractures and coronae of Parga Chasmata (unit fchP) is composed of materials related to Kulimina Corona, Hervor Corona, Xmukane Corona, and an unnamed nova (lat 27.5° S., long 267.5° E.) located inside Parga Chasmata. Some of the flows are related to Parga Chasmata and flow out of graben and fractures of the fracture belt. Unit fchP covers most of the northern map area, forming a large flow field composed of multiple flows that have varying radar backscatter, flow direction, and origin. The western part of unit fchP is composed of a series of large flows containing different textural characteristics that could be explained by a change or evolution of material composition or by emplacement conditions. Large flows show a range of backscatter character and texture: (1) flows that contain dark margins, which provide evidence of changes in flow condition during emplacement or post-emplacement modification of the interior of the flow (inflation of the sheet flow; Byrnes, 2002), (2) flows that have bright margins, which are considered the result of the deformation of the flow during advance (Byrnes, 2002), and (3) composite subparallel and polylobate flows that have hummocky texture. Some flows display a texture that appears related to flow emplacement and is perpendicular to the estimated flow direction. Other flows display a large ropy structure (lat 27.5° S., long 247° E.) that helps to constrain the flow direction to the west.

The eastern part of unit fchP is composed of flows that extend more than 1,000 km to the south and southwest. The flows display channels as much as ~170 km long parallel to flow direction. Some flows show a change in flow direction around previously formed structures (Oanuava Coronae and Achall Corona) or locally fill the inner lows of previously formed structures, indicating local topographic control of flow emplacement. High-backscatter flows that seem to emanate from fractures and graben of Parga Chasmata and flow for distances greater than 350 km in the same direction are emplaced over the channel-fed flows. The youngest flows of unit fchP form a group of flows of high-backscatter and lobate morphology that surround the large tectonomagmatic features located in Parga Chasmata: Hervor, Xmukane, and Kulimina Coronae and an unnamed nova. Some of the flows display central leveed channels. Many of the flows related to these large features are intertwined, making it impossible to define individual units; however, one tectonomagmatic feature, Kulimina Corona, seems to be the main source for the materials that form unit fchP. In addition to these large flows, numerous medium and small volcanic features occur in unit fchP. Medium-size volcanoes are partially covered by unit fchP flows, and small shields that occur across the unit and have steep-sided domes are concentrated in the interior of the coronae. Temporal relations between unit fchP and the surrounding materials are locally constrained, but these relations cannot be extrapolated across the map area due to the regional extent and composite nature of unit fchP. Local relations between unit fchP and the basement are constrained, because basement units are located higher than the surrounding materials and host tectonic

structures are covered by the younger flows. Distal flows of unit fchP locally embay unit tu, and flows of unit fchP embay and cut unit Pa, unit Pb, and unit Pc. Temporal relations with other volcanic units of the PCR are more difficult to determine. Unit fchP fills the interior and embays radial structures associated with an unnamed corona located in unit fsZ, indicating that local flows of unit fchP postdate the eastern part of unit fsZ. This relation does not apply to the whole unit, because shield-related materials in the western part of unit fsZ postdate unit fchP. Northwest-striking fractures, which dominate the northwestern map area, cut unit hu and are locally embayed by distal materials of unit fchP, indicating that part of unit fchP locally postdates part of unit hu. Due to the composite nature of both units, this temporal relation cannot be applied to the rest of the PCR. Unit fchP correlates with the unit flow materials unit 2 of Chapman (1999, unit f_2, V–40). The materials of unit fchP associated with Hervor and Xmukane coronae and the unnamed nova in the map area are mapped in the Galindo quadrangle (V–40) to the north as a separate unit called corona material, undivided, of Chapman (1999, unit co). The intertwined character of the corona-related flows associated with Parga Chasmata makes correlating the unit from V–52 to V–40 difficult. In V–40, Chapman's correlative unit is interpreted as regional materials that form part of the planum, which represents material that predates the emplacement of corona-related units related to Parga Chasmata; in V–52, we interpret unit fchP as corona- and chasma-related materials.

Flow material from Oanuava Coronae and Achall Corona (unit fc0A) consists of a composite unit formed by sheet flows of moderate to high backscatter. Unit fc0A completely surrounds Oanuava Coronae, Achall Corona, and other smaller volcanic features. West of Oanuava Coronae, unit fc0A shows digitate terminations and mottled radar texture in the proximity of the source. Most of unit fc0A shows a characteristic kilometer-scale, reticulate texture that marks the limit of the unit where radar contacts are not clear. East of Oanuava Coronae, unit fc0A is more difficult to distinguish from its surroundings, although flow directions to the southeast help delineate the unit limit. Some small flows of variable backscatter southwest of Oanuava Coronae may originate from the corona annulus. Other volcanic features that might provide sources for unit fc0A include a steep-sided dome (lat 34.8° S., long 256.8° E.) southeast of Oanuava Coronae and a caldera-like structure (lat 34.9° S., long 253.4° E.) southwest of Oanuava Coronae. The caldera-like structure displays concentric pit chains, possible evidence of subsurface dikes or dilational normal faults (for example, Okubo and Martel, 1998; Bleamaster and Hansen, 2001; Ferrill and others, 2004; Schultz and others, 2004). Shields occur as groups or in isolation within unit fc0A; clusters of small- to medium-size edifices in the interior of Oanuava Coronae and Achall Corona may represent a late volcanic episode associated with corona evolution. Unit fc0A postdates the local basement materials; units tu and Pa form kipukas. Unit Pa is in contact with the westernmost limit of unit fc0A; flows of fc0A overlap unit Pa, although, locally, contact relations are masked by small shields. Temporal relations between unit fc0A and other PCR units are difficult to establish. In northernmost unit fc0A, materials of fsZ are covered by the corona-related flows. These temporal relations cannot be extrapolated to the whole contact between unit fsZ and unit fc0A, because flows of unit fsZ related to the shield field located at lat 29° S., long 254° E. are locally emplaced over the materials of unit fc0A. The relations between unit fc0A and unit hu are constrained along the west boundary of unit fc0A where a long channel that cuts unit hu is clearly embayed by the distal edge of unit fc0A, indicating that, locally, unit hu predates unit fc0A. The extensive corona-related unit fc0A and unit fchP interact in different locations in the northern map area. In northeasternmost unit fc0A, flows of fchP locally fill the interior of Achall Corona and also embay local structures related to the corona. In other locations (for example, west boundary of unit fc0A), distal materials of this unit postdate flow fronts of unit fchP.

Flow material from Lalohonua Corona (unit fcL) is composed of a series of flows that originated in Lalohonua Corona, a 450-km-diameter asymmetric corona located in the Galindo quadrangle (V–40; Chapman, 1999). The longest flows of unit fcL are sheet-like flows that have homogeneous intermediate backscatter. The presence of a long channel (~120 km) that contains flows at its termination could indicate a channel-fed origin for these flows and could help to constrain a southwestern flow direction. Near Lalohonua Corona, unit fcL is composed of multiple, medium to high backscatter, lobate flows that flow radially from the corona towards the south and the southeast. Some lobes host central leveed channels, indicating that these flows are also channel fed. Flows of unit fcL postdate unit fchP. Unit fcL correlates with corona materials of Chapman (1999, unit m, co_m) in Galindo quadrangle (V–40), where the corona source of the materials is located.

Flow material from Hlineu Corona (unit fcH), located in the westernmost map area adjacent to Imdr Regio quadrangle (V–51), is a corona-related unit composed of materials of homogeneous intermediate to low backscatter that originated in Hlineu Corona. Some materials of unit fcH probably also emerged from small volcanic edifices near the corona. Unit fcH includes a series of sheet flows of homogeneous texture that flowed to the east. We infer flow direction from the interaction of flows and a fracture set located east of the corona near Chuginadak Mons. The interaction of flows with fractures in some locations also indicate that unit fcH postdates part of unit hu; as with other previously described units, this relation is not applied to the whole unit due to the composite character of unit hu. A crater halo in the western map area further obscures delineation of unit contacts.

Flow material from Witte Patera (unit fpW), located in the northern map area along the boundary with the Galindo quadrangle (V–40), is composed of multiple flows of intermediate to high backscatter that are radial to the central, ~50-km-diameter, circular volcanic Witte Patera. Numerous, overlapping flows fed by leveed channels extend radially from the central source for 50 to 100 km and have lobate fronts that delineate the contact between unit fpW and the surrounding materials. Lobate flows of unit fpW postdate unit fchP and the parts of unit hu where they are in contact. Temporal relations between unit fpW and unit fcL are best constrained in the Galindo quadrangle (V–40), where the materials of unit fcL (corona-related unit co of Chapman, 1999) postdate unit fpW.

Flow material from Destinnová Patera (unit fpD) is composed of materials of intermediate backscatter and homogeneous texture that flow from Destinnová Patera, a small (30 km-diameter) caldera marked by a central depression and a set of concentric fractures. Flow lobes and lobate edges indicate flow direction and extent. Unit fpD flowed to the north for more that 140 km. Another suite of small radial flows (15–20 km long) surrounds the caldera. Concentric fractures of the caldera cut these radial flows, yet the flows also locally overprint the concentric fractures, indicating that the caldera formed contemporaneously with emplacement of the flows. The flows of unit fpD locally overlap units hu, fchP, and fc0A, but these local temporal relations cannot be extrapolated beyond this area.

Flow material around Azimua Tholi (unit ftA), located between impact craters Kanik and Rose, includes materials of high backscatter and reticulate to mottled texture. Two possible sources can be established for unit ftA: two nested, steep-sided domes (Azimua Tholi) around which the materials are disposed and a concentric set of fractures that forms a caldera-like structure located north of the unit. Flows of unit ftA embay the nested domes. The easternmost dome apparently experienced lateral flank collapse, which disrupted its original morphology. This dome hosts collapse-related deposits: (1) proximal facies composed of homogenous bright materials that have lineaments parallel to the original scarp and (2) distal hummocky terrain facies composed of blocks <5 km across. Many small shields also occur on unit ftA, so a contribution of point-sourced volcanism to unit formation should be considered. Unit ftA postdates a volcanic channel that formed in unit hu, suggesting unit ftA locally postdates parts of unit hu.

Flow material from Monoshi Tholus (unit ftMo) is composed of materials of mottled texture and intermediate backscatter disposed around Monoshi Tholus, a flat-topped tholus with a summit caldera. Monoshi Tholus displays a steep western slope and a gradual eastern slope. Unit ftMo displays flow fronts to the northwest and south and hosts numerous small shields. Unit ftMo postdates the materials of unit tu, but the contact between units ftMo and hu is approximate.

Shield field and associated materials near Monoshi Tholus (unit sfMo), spatially related to unit ftMo, are composed of shield-related materials of medium backscatter that form an areally discontinuous layer due to the point-sourced nature of the shield-related processes. Shield characteristics include shields with or without summit pits and large edifices with summit calderas. Kipukas of unit tu appear within unit sfMo, predating the emplacement of the shield-related materials. Temporal relations with the surrounding units fc0A, ftMo, and hu are difficult to establish due to the discontinuous nature of unit sfMo, although the presence of shields on the surrounding materials could indicate that the emplacement of the shields that form unit sfMo also postdated the other units. The contact between unit sfMo and units fc0A, ftMo, and hu is mapped as gradational or approximate to express the uncertainties of these relations.

Shield fields and associated materials around Sitapi Coronae (unit sfSi), in the northwestern map area, consist of heterogeneous shield-related materials of different backscatter and texture. Shields form clusters with different characteristics; shield densities show no correlation with topography. Some shield clusters are related to Sitapi Coronae, but most show no obvious association with large tectonomagmatic features. Shields associated with Sitapi Coronae are parallel to a set of north-striking fractures. In the northwestern part of unit sfSi, shield-related material covers regional northwest-striking fractures; although, locally these fractures cut some shield-related materials, indicating time-transgressive relations of shields and fractures or structural reactivation of the fractures. The relations between shields and fractures suggest a structural control on shield emplacement. Individual shields within the clusters display different morphologies, including pits surrounded by flows of the same backscatter, mounds without pits, flat-topped shields with and without pits, and cone-like morphologies. Most edifices are ≤10 km in diameter, but some isolated shields are >10 km diameter. We consider unit sfSi a point-sourced, composite unit, comprised of different shield formation episodes of different age and nature. This point-sourced and locally discontinuous nature results in local gradational contacts with surrounding materials. Unit sfSi cannot be used as a temporal reference for surrounding units, although it embays basement units tu and Pa in the northwestern map area and locally postdates units hu and fcH.

Sequence of Materials in the Helen Planitia Region

The HPR in southern Helen Planitia quadrangle (V–52) is dominated by regionally distributed, north-striking fractures and radial and concentric structures associated with coronae and radial fracture systems. Most of the coronae show spatial correlation with regional fracture systems, but large flow units—similar to those associated with PCR coronae (for example, Oanuava and Hlineu Coronae)—cannot be delineated with confidence. This apparent absence of large flows does not necessarily mean that these coronae lack large flows; flows could have homogenized due to weathering processes (Arvidson and others, 1992) to become part of the heterogeneous material. The HPR includes several major units, including basal Helen Planitia materials overlain by shield- and volcano-related flows and heterogeneous materials (pHu, sfSo, fmN, fmA, sfE and fsU).

In western HPR, the basement of tessera terrain and Helen Planitia materials occurs topographically higher than surrounding materials and predates an assemblage of heterogeneous and shield-related materials.

Helen Planitia materials, undivided (unit pHu), preserved in large outcrops located within broad topographic highs (for example, Tsovinar Dorsa) and in several kipukas, comprise materials of intermediate to high backscatter, which contain textures that vary from homogeneous to a kilometer-scale reticulate pattern. A bright parabolic halo related to impact crater Adaiah mantles much of southeastern HPR and obscures the original backscatter and texture, in part, of unit pHu. No primary structures are preserved within unit pHu, but many shields and associated materials lie stratigraphically above unit pHu. Whether shield-related volcanic activity contributed to unit formation or shields resulted from discrete shield formation events

that postdated emplacement of unit pHu is unconstrained. The point-sourced nature of the shield-related materials emplaced in or on unit pHu and the surrounding units and the presence of the crater halo obscures some of the contacts with adjacent materials, as shown by approximate contacts. In the outcrop centered at lat 41.5° S., long 252° E., two local orthogonal fracture and graben suites cut unit pHu but do not cut the overlying material, which provides temporal constraints. Where unit pHu is in contact with tessera terrain material, clear embayment relations indicate that unit pHu postdated unit tu. All basement units are, in turn, embayed by unit hu.

In eastern HPR, the largest outcrop of unit pHu occurs in the interior of a large circular structure (lat 39.5° S., long 262.5° E.). Other outcrops of unit pHu form isolated patches partially covered by young, shield-related materials. The relation of pHu with unit tu in eastern HPR is unconstrained due to the lack of clear contacts. In the transition area between PCR and HPR regions, flows of unit fmM postdate materials of unit pHu.

Although shields or groups of shields occur in almost all of the units across the HPR, there are areas where these volcanic features and their associated materials coalesce to form a distinctive unit. In these locations, the large number of edifices and the likelihood of additional shields below image resolution probably result in an underestimated number of shields. Shield field and associated materials near Sopdet Tesserae (unit sfSo) are geographically related to unit tu in the northwest-trending elevated swaths of basement terrain of western HPR. Unit sfSo is composed of shields and shield-related flows of intermediate backscatter and reticulate texture that form a layer above the local tessera terrain. A subtle northwest-trending tectonic fabric in association with unit sfSo likely indicates the incomplete burial by shields or structures within the underlying unit tu, or it is a product of structural reactivation of these same structures. Unit sfSo surrounds small kipukas of unit tu and embays the large inliers of tessera terrain. The contact between units sfSo and hu is difficult to establish in some locations due to the discontinuous character of the point-sourced shield material and the presence of shields in unit hu. In the western map area, unit sfSo postdated unit fcH along its southern limit, located in the transition between PCR and HPR.

Flows and shield-related materials around Ustrecha Tesserae (unit fsU), which cover much of eastern HPR, form a composite unit of corona- and volcano-related flows that are discontinuously covered by shields and shield clusters composed of intermediate to low backscatter materials that have a heterogeneous texture. Unit fsU postdated formation of the HPR basement. Some shield clusters are isolated, but others are spatially related to large tectonomagmatic features or to regional and local fractures sets. The point-sourced nature of the shield-related material makes unit fsU a locally discontinuous unit. The contact of unit fsU with surrounding units is approximate and (or) gradational. Units tu and pHu are embayed by the shield-related materials and individual shields also present in the basement materials. The locally discontinuous nature of unit fsU reveals underlying basal materials of unit pHu. Temporal relations between units fsU and hu are difficult to establish due to the composite and time-transgressive nature of both units, as well as the presence of shields in each unit. Along the HPR-PCR boundary, materials of unit fmM were emplaced over unit fsU materials.

Shield fields and associated materials in Enekeler Corona (unit sfE), located in the interior of Enekeler Corona in eastern HPR, include multiple shields and shield-related flows that display intermediate backscatter and a heterogeneous local reticulate texture produced by the point-sourced nature of the unit. Shields display different morphologies, and pitted mounds dominate. Shield clusters and related flows coalesce to form locally continuous patches that cover the corona interior and part of the surrounding area. If unit formation is related to this large tectonomagmatic structure, it presumably represents a late episode of corona evolution. Unit sfE is emplaced over and, therefore, postdates units tu and fsU. Unit sfE embays small kipukas of unit tu inside Enekeler Corona. The contact of units sfE and fsU is shown as approximate due to the shield-related nature of both units. Where clear contact relations exist between these two units, the material of unit sfE postdates material of unit fsU; but, due to the composite character of unit fsU, this local relation is not extrapolated across the HPR.

Flow material fron Ne Ngam Mons (unit fmN), located in central HPR, locally postdated unit hu. Unit fmN shows long, intermediate-backscatter flows that form the outer apron of Ne Ngam Mons and low-backscatter flows that form the inner slopes of the edifice. Both sets of flows are radial to a central summit caldera. The longest flows extend to the southeast; some northwest-trending flows fill the interior of a nearby unnamed corona and embay two steep-sided domes that formed in the corona annulus. Mechanisms of emplacement for the intermediate-backscatter flows are unconstrained, but the low-reflectivity flows display a 50-km-long channel- or tube-like structure on the east flank of the volcano. Shields and a small dome on the summit of Ne Ngam Mons, probably part of the late evolution of the volcano, are also part of unit fmN. The materials of unit fmN interact with a suite of regional north-striking fractures; intermediate-backscatter flows predated the fractures, which are partially covered by younger flows.

Along the boundary with the Themis Regio quadrangle (V–53) east of the map area, low to intermediate backscatter materials that form the unit flow material from Abeona Mons (unit fmA) are composed of distal flows of Abeona Mons (lat 44.8° S., long 273.1° E.), a 375-km-across, steep-sided dome located in southwestern V–53. Unit fmA embays unit tu. Temporal relations between unit fmA and unit fsU are unclear due to the heterogeneous character of the shield-related unit, similar backscatter character of both units along their contact, and the presence of scattered shields in both units.

Tectonic Structures

The Helen Planitia quadrangle (V–52) displays a variety of secondary structures that variably deform almost all units. Tectonic structures include (1) structures associated with tessera terrain, (2) regional deformation, (3) local structural suites related to tectonomagmatic features, and (4) localized deformation.

Structures Associated with Tessera Terrain

Tessera terrain inliers in the map area preserve different patterns of intersecting structures: ribbons, fractures, graben, and folds. Temporal relations of deformation between inliers are unconstrained due to the absence of mutual contact relations and the lack of similar structural fabric orientation. Ribbon-like structures, comprised of parallel, alternating, kilometer-wide ridges and troughs (Hansen and Willis, 1996, 1998), occur in some inliers of unit tu. Ribbon trends vary from inlier to inlier, lacking coherent patterns across the map area. Northwest-trending ribbons deform inliers of unit tu, located at lat 39° S., long 248.5° E. and lat 50° S., long 263° E., that have a constant ribbon wavelength of 2–2.5 km, suggesting a shallow depth to the brittle-ductile transition (BDT) at the time of ribbon formation (Hansen and Willis, 1998) or a shallow depth to a solid-liquid phase transition (Hansen, 2006). In other tessera terrain inliers, ribbons are deformed, are embayed by younger flows, or show evidence of reactivation; original ribbon characteristics are indeterminate (for example, inlier of unit tu located at lat 35.5° S., long 258° E.). In the inlier of unit tu located at lat 50° S., long 263° E., northeast-trending 5–10-km-wavelength folds trend orthogonal to ribbons. Fold wavelength indicates an increase in layer thickness as compared with the thickness for the time of ribbon formation (Hansen and Willis, 1998; Brown and Grimm, 1997; Ghent and Hansen, 1999; Hansen and others, 1999; Hansen, 2006).

In Sopdet Tesserae, closely spaced northwest-trending fractures and ridges deform the materials of unit tu. North-northeast-trending fractures and graben cut the northwest-trending fractures and ridges. All other tessera terrain inliers display an intricate pattern of intersecting lineaments (for example, local radial patterns in Ustrecha Tesserae). East- and northeast-trending graben and arcuate graben displayed in Sopdet Tesserae represent the last deformation events recorded in the tessera terrain inliers. Graben, embayed by younger volcanic materials of low backscatter, range in width from 2 to 6 km and display coherent trends and characteristics across the map area, although temporal relations between inliers are elusive.

Regional Deformation

Fold Belts and Wrinkle Ridges

Two different styles of contractional deformation occur in Helen Planitia quadrangle (V–52): deformation belts (dorsa) that show concentrated strain and subparallel, regional wrinkle ridges that record distributed strain. Tsovinar Dorsa, a northwest-trending 1,100-km-long anastomosing Class II deformation belt (Banerdt and others, 1997), connects Tangba Corona with an inlier of unit tu and marks the north edge of Helen Planitia. The deformation belt varies in width along strike, displaying bottleneck morphology and a division into two different branches at lat 46.2° S., long 254° E. Fold characteristics include lengths from 10 to 100 km and wavelengths from 5 to 10 km. Different fold morphologies are distributed along Tsovinar Dorsa: folds that show width variation along trend and complex, broad folds that have superposed, parallel, smaller-wavelength folds. The other broad topographic ridge, Kastiatsi Dorsa, which extends about 1,200 km into V–60 to the south, lacks contractional structures like those developed in Tsovinar Dorsa. Kastiatsi Dorsa is a broad, northeast-trending warp that, combined with Tsovinar Dorsa, forms a circular topographic arch that dominates northern Helen Planitia.

Various suites of wrinkle ridges deform lowland materials, as well as corona- and volcano-related materials, that reside above the mean planetary radius (6,051.84 km) near Parga Chasmata (fig. 3, map sheet). In the southeastern map area, north-northeast- and north-northwest-trending wrinkle ridges reflect the main deformation trends; locally, this trend is modified around coronae-paralleling local annuli (for example, Enekeler Corona). The wrinkle ridges display variable spacing and length. This wrinkle-ridge suite is part of the regional circum-Themis trend, presumably formed in response to lithospheric loading of Themis Regio (Billoti and Suppe, 1999). In the western map area, northwest-trending wrinkle ridges mark the regional Helen Planitia trend (Billoti and Suppe, 1999), where wrinkle ridges trend parallel to the geoid contours defined by Sandwell and others (1997) and are likely related to formation of Themis Regio. The wrinkle ridges, spaced 2 to 20 km apart and having lengths of 5 to 50 km, deform a wide range of materials, including units pHu, sfSo, sfSi, fcOA, fmA, and hu. Locally, shield-related materials of unit hu pooled along wrinkle ridges, suggesting that the emplacement of some materials of unit hu and (or) wrinkle-ridge formation formed diachronously.

North-trending wrinkle ridges extend over the central Helen Planitia quadrangle. Contrary to the north-northeast- and north-northwest-trending wrinkle-ridge suites that are related to regional trends (Billoti and Suppe, 1999), this wrinkle-ridge suite appears to be locally restricted to the map area. Although Billoti and Suppe (1999) described a regional change in wrinkle-ridge orientation west of the map area in Imdr Regio (V–51; lat 43° S., long 212° E.), we propose that Helen Planitia quadrangle displays two distinct trends of wrinkle ridges rather than a change in trend. Locally, north-trending wrinkle ridges parallel north-striking fractures and have a morphological transition from fractures to wrinkle ridges along strike. In locations where this transition occurs, flows covered the fractures prior to wrinkle-ridge formation. Similar observations led to a model for the formation of the wrinkle ridges that includes filling of previous fractures by flows and subsequent reactivation as inversion structures under the appropriate stress conditions (DeShon and others, 2000; Hansen, 2005). Because the existence of previous, covered fractures and wrinkle ridges is locally constrained, formation of the entire north-trending wrinkle-ridge suite as inversion structures cannot be established, although it might be possible. North-trending wrinkle ridges deform units Pa, fcH, fcOA, fchP, fpD, ftMo, sfSi, sfMo, and hu.

Another local northeast-trending wrinkle-ridge suite in the eastern map area deforms unit Pc. At lat 32.8° S., long 269.4° E., two scales of ridges occur: closely spaced (<2 km), northeast-trending, small ridges and northeast-trending wrinkle ridges spaced 5–15 km apart. To explain the occurrence of both parallel ridge suites, mechanical considerations are taken into account. Assuming that the spacing of structural suites reflects

the thickness of the deformed layer (for example, Ramberg, 1955; Talbot, 1970; Price and Cosgrove, 1990; Pollard and Aydin, 1988), then the short- and long-wavelength ridges could indicate thin and thick layers, respectively, that were deformed within a single event. Both suites could also result from progressive thickening of a deformed layer through time, showing a temporal transition from short- to long-wavelength deformation. Whether ridge suites formed synchronously through deformation of thin and thick mechanical layers or as a result of a temporal change of layer thickness is unconstrained. At lat 41° S., long 267.5° E., the long-wavelength, northeast-trending wrinkle-ridge suite is cut by the north-northwest-trending, circum-Themis trend and defines a local polygonal pattern.

Regional Fracture Suites

Northwest-striking, parallel fractures and graben cut units Pa, hu, fcH, and sfSi in the northwestern map area (fig. 4, map sheet). Fracture characteristics include 1–4 km spacing, lengths of 5–200 km, and widths <1 km. A spectacular case of fracture reorientation occurs around Sitapi Coronae, where the northwest fracture trend is completely reoriented to form a suite of east-trending fractures and graben that cuts units hu, sfSi, and ftMo. The length of the east-trending fractures and graben ranges from 40 to 500 km, and spacing between structures is from 2 to 35 km. The east-trending fractures display undulating morphology, shear component, and variation in width along strike. Other characteristics, such as en echelon terminations, pits, pit chains, and alignment of shields along the fractures, provide evidence for subsurface dikes or dilational normal faults (Okubo and Martel, 1998; Schultz and others, 2004; Ferrill and others, 2004). Local modifications of the northwest trend also occur around a shield cluster of unit sfSi, located at lat 33.8° S., long 244° E, where fractures bend around the shield cluster. Shields and shield-related flows locally cover the fractures, although fractures also cut shield-related materials, which indicates broadly contemporaneous shield and fracture formation.

A north-striking fracture suite, locally modified to north-northeast and north-northwest trends around large tectonomagmatic features, dominates the southern map area (fig. 4, map sheet). Most structures form single, radar-bright lineaments, interpreted as extension fractures, that are obvious in both left- and right-illumination images. Paired opposing lineaments (width <1 km) are interpreted as graben. Fracture length varies from 3 to 150 km. Fracture spacing varies in the southern map area from close spacing (<2 km) within fracture belts (for example, Ajina Fossae; lat 45° S., long 258° E.) to 5- to 10-km-spaced fractures between fracture belts. Fracture belts connect and interact with different tectonomagmatic features (for example, Ajina Fossae connects Ne Ngam Mons and Tangba Corona), suggesting a possible genetic association of large tectonomagmatic features and fracture belts. The interaction between the regional stress fields responsible for regional fractures and the local stress fields associated with local tectonomagmatic features could produce deviations in fracture orientation adjacent to the tectonomagmatic features. The regional north trend of the fracture suite is modified along Kastiatsi Dorsa, where fractures parallel the arcuate northeast trend of the broad warp. Flows and shield-related materials of unit hu locally cover north-striking fractures; shields cover fractures and fractures cut shields, indicating that fracture and shield formation was diachronous. Shield clusters on units sfSi and fsU are also related to fractures, which may control shield emplacement and produce local fracture reorientation around the shield clusters.

An approximately 2,000-km-long and 600-km-wide section of Parga Chasmata dominates northern Helen Planitia quadangle. This 10,000-km-long fracture belt includes twelve branches (Stofan and others, 2000), two of which—a main branch that dominates the northeast and a smaller branch centered at lat 28.5° S., long 254.5° E.—occur in the map area. The distribution of tectonic features that form the chasmata is not uniform; structures concentrate in the vicinities of large coronae and nova. The chasmata may represent the spatial and temporal interaction of different processes that contribute to tectonomagmatic feature formation. Tectonic features of Parga Chasmata include graben, fractures, and linear scarps interpreted as faults. Most lineaments follow the west-northwest trend of the chasmata, although some lineaments trend east and northeast around local tectonomagmatic features. A suite of north-northwest-trending, regularly spaced (<1.5 km), single, straight lineaments 3–50 km long are interpreted as fractures. These fractures represent an early fracture suite, shown by crosscutting relations of corona-related flows and other chasmata-related structures. The predominant structures of Parga Chasmata are graben, marked by parallel-paired lineaments that display straight or sinuous traces and en echelon morphologies. The graben are generally <2 km wide, range from 3 to 40 km long, and are spaced 1–3 km apart. Individual lineaments, interpreted as extension fractures, are associated with the graben that have similar length and spacing. Extension fractures are concentrated in chasmata troughs in the branch of the chasmata located at lat 28.5° S., long 254.5° E. Linear radar-bright scarps, interpreted as fault scarps, are located in central and eastern Parga Chasmata, around Kulimina Corona, and in an unnamed nova (lat 27.5° S., long 267.5° E.). These scarps, interpreted as normal faults, range from 2 to 50 km in length and typically face southwest parallel to the fracture zone. Faults around Kulimina Corona, spaced <2 km apart, merge with the corona annulus.

Parga Chasmata was an active fracture belt during most of the time represented by the materials in the northern map area. Fractures and graben of Parga Chasmata cut units Pa, Pb, Pc, ftO, fsZ, fcOA, fchP, fpW, and fcL. In most of these units, the materials postdate, but are also cut by, the structures of Parga Chasmata, suggesting that tectonism accompanied surface material emplacement.

Local Structural Suites Related to Tectonomagmatic Features

Magmatic and tectonic processes associated with large tectonomagmatic features such as coronae and novae played an important role in the geological evolution of Helen Planitia quadrangle (V–52). Fourteen well-defined coronae that have diameters of 100–375 km, five large structures whose clas-

sification is problematic, and two novae are distributed across the map area. The large tectonomagmatic structures in the map area show a strong spatial correlation with Parga Chasmata and other smaller deformation belts (for example, Ajina Fossae). We define two different groups of structures on the basis of their association with these fracture belts: structures spatially associated with Parga Chasmata and structures outside Parga Chasmata.

Tectonomagmatic Structures Related to Parga Chasmata

Six coronae and an unnamed nova are spatially associated with Parga Chasmata (fig. 4, map sheet): Oanuava, Achall, an unnamed corona (lat 28.5° S, long 258° E.), Kulimina, Hervor, Xmukane, and an unnamed nova (lat 27.5° S., long 267.5° E.). These tectonomagmatic structures interact among each other and with the chasmata structures, suggesting broadly synchronous formation of the coronae and the chasmata. Coronae associated with Parga Chasmata display three suites of structures: radial fractures, concentric fractures, and fault scarps. Most coronae host both radial and concentric fractures, but fault scarps form part of the annulus only in Xmukane Corona and appear restricted to chasma-related structures in the interior of Kulimina Corona. Radial fractures, presumably formed during domical uplift and (or) dike emplacement related to corona formation (Janes and others, 1992; Squyres and others, 1992; Stofan and others, 1992; Koch and Manga, 1996; Ernst and others, 1995) are preserved in Oanuava, Achall, Kulimina, and Xmukane Coronae. Xmukane Corona, a hybrid feature between a corona and a radial fracture system, displays radial fractures in its entire perimeter that postdated the adjacent Hervor Corona. In the unnamed corona and Achall Corona, portions of the radial fracture suites are covered by corona-related flows from Kulimina Corona. All coronae associated with Parga Chasmata display annuli marked by concentric fractures, although the morphology and degree of preservation varies between coronae. In Oanuava Corona, three different sections of concentric suites of fractures surround the tectonomagmatic feature and compound the complex annulus of the composite corona. Fractures of the complex annulus cut unit fcOA, although sections of the annulus are also postdated by part of unit fcOA, suggesting broadly synchronous formation of the annulus and corona-related volcanic activity. Hervor Corona annulus, marked by two concentric structural suites, displays a double-ring morphology. A third smaller concentric annulus, spatially coincident with a topographic low in the corona interior, postdated formation of the inner fracture ring. All structural suites postdated the materials of unit fchP, some which were emitted by Hervor Corona, and are cut by graben and fractures of Parga Chasmata. The annuli of Chanum, Achall, and Kulimina Coronae are partially flooded by chasmata- and corona-related flows of unit fchP and also are cut by fractures and graben of Parga Chasmata. Graben and scarps of Parga Chasmata merge with the annulus of Kulimina Corona.

Radial fractures of Xmukane Corona and the unnamed nova deform units Pb and fchP. The radial fractures cut the graben of Parga Chasmata but are also cut by fractures and scarps that form part of the chasmata-related fracture belt, indicating contemporaneous evolution of both structures and the chasmata. Radial fractures of the nova are interdigitated with the radial fractures of Xmukane Corona, and mutual temporal relations are unconstrained.

Tectonomagmatic Structures not Related to Parga Chasmata

Local fracture trends associated with tectonomagmatic features outside Parga Chasmata deform, and interact with, many different units. Contrary to relations in Parga Chasmata, these tectonomagmatic features are dispersed, inhibiting relative temporal interpretations. In addition, with the exception of Hlineu Corona, extensive corona-related flow units associated with coronae are not obvious—perhaps they are the result of homogenization processes that could mask evidence of extensive flows (Arvidson and others, 1992). These tectonomagmatic features are separated into two categories: features associated with north-trending regional fracture suites and isolated features (fig. 4, map sheet).

Hlineu, Sitapi, Nungui, Tangba, and an unnamed corona (lat 42° S., long 256.5° E.) are all associated with a suite of north-striking regional fractures. Two local structural suites relate to these coronae: radial and concentric fractures. Radial fractures occur in western Sitapi Coronae but are not recognized in the other coronae; they might never have formed, or they might be buried by subsequent corona-related volcanism.

Concentric fracture suites define the annuli of all the coronae, although each annulus is different and records histories not related to individual units. The annulus of Sitapi Coronae, slightly elongated along a northwest-southeast axis and marked by fractures and graben, postdates radial fractures and the regional east-trending fracture set, which is a result of the reorientation around the corona of the northwest-trending regional fracture system. North-striking regional fractures postdate the annulus, partially covered by the shield-related materials of unit sfSi. Hlineu Corona displays an asymmetric annulus that is open to the north and composed of graben and fractures. Annulus fractures postdate the materials of unit fcH, indicating that part of the process of annulus formation occurred after emplacement of extensive corona-related flows. North-striking regional fractures cut some annulus fractures but are also cut by other annulus-related structures, suggesting multi-stage annulus formation. Northwest-striking regional fractures in the western map area merge with the annulus of Hlineu Corona; temporal relations between both structural suites are difficult to establish. Nungui and Tanga Coronae display concentric, double-ringed annuli composed of fractures and graben, which formed in conjunction with north-trending regional fractures that deform the local materials of unit hu. These regional fractures postdate the outer annulus of Nungui Corona but do not affect the inner ring of fractures. Nungui Corona annulus is incomplete in the south; however, it is not clear if this relates to emplacement of, and burial by, shield-related material of unit hu or is the result of incomplete annulus formation. The interior of the corona, free of fractures, displays a shield cluster that locally buries the fractures, although fracture density due to strain partitioning around the corona cannot be ruled out. Tangba Corona displays a slightly elongated annulus along a

north-south axis that is wider in the west than in the east. The western rim of the corona tilts to the east. Regional north-striking fractures cut concentric rings of structures north and south of the corona and merge with the annulus in the east and west. North-northeast-trending wrinkle ridges of the circum-Themis Regio trend (Billoti and Suppe, 1999) also cut the southern part of the annulus.

The unnamed corona (lat 42° S., long 256.5° E.) displays a concentric annulus that cuts unit hu and interacts with volcano-related flows of unit fmN. Flows of unit fmN fill the corona interior, but some concentric fractures of the corona annulus cut the flows, which implies that the formation of the corona annulus occurred, at least in part, during emplacement of unit fmN. Two steep-sided domes that represent a late magmatic event presumably associated with corona evolution postdate the corona annulus, which is also cut by north-striking fractures and by radial fractures centered at lat 40.3° S., long 257.8° E.

Enekeler Corona, an isolated asymmetric corona characterized by an irregular topographic signature, displays a poorly defined annulus, composed of concentric ridges in the south and fractures in the northeast that deform shield-related materials of unit fsU, but is obscured by multiple clusters of shields and the associated materials of unit sfE. The northern part of the feature is cut by north-striking fractures that are covered in the interior by shield-related materials of unit sfE. North-northwest-trending wrinkle ridges of the circum-Themis trend are deflected around the corona and merge with the southern section of the annulus.

Chanum Corona, spatially associated with the northwest-trending regional fracture suite, displays a double concentric annulus of fractures in the south and a small section barely visible in the north. The fracture annulus cuts unit hu, but shield-related materials of unit hu postdate sections of the annulus. Northwest-striking fractures that cut the annulus are locally reoriented to north-striking fractures in the southern part of the corona. Some north-striking fractures south of the corona could be early-formed, radial fractures of the corona. A shield field in the corona interior postdated the northwest-striking fractures.

The group of tectonomagmatic features unrelated to regional fracture trends includes two coronae, Mertseger Mons, and three features of unclear classification. Three suites of structures, radial fractures, concentric fractures, and concentric ridges, are related to these features, although not all are related to the individual tectonomagmatic features.

Two structures, Mertseger Mons and a large unnamed tectonomagmatic structure (lat 40° S., long 263° E.), are characterized by a radial suite of fractures and graben. Mertseger Mons, a 450-km-diameter nova, displays a suite of radial fractures and graben that terminate in extensive flows of low backscatter. The association between fractures, graben, and flows suggest that these radial structures reflect a surface manifestation of dikes. The transition from graben to fissures and fractures, the presence of flows at the fracture termination, and the presence of northwest-trending pit chains that seem related to this large tectonomagmatic structure also support the presence of dikes associated with Mertseger Mons. The unnamed tectonomagmatic structure, whose topographic signature is a large topographic rim, displays radial and concentric fracture suites located within the topographic rim (unit pHu). Radial fractures and graben are distributed along the perimeter of the feature; whereas, concentric fractures are restricted to the northeastern part of the structure where they cut radial fractures and graben. The interior, and much of the annulus, is covered by unit pHu and shield-related materials of unit fsU.

The unnamed corona (lat 41.6° S., long 265.5° E.) displays an incomplete circular annulus, formed by two concentric rings of fractures and ridges, that is absent in the northern and southern parts of the corona. North-northwest-trending wrinkle ridges of the circum-Themis trend (Billoti and Suppe, 1999) merge with the corona structures that form the western annuli. Shield-related materials of unit fsU cover annulus structures but are also cut by local corona-related fractures.

Three structures, Nordenflycht Patera and two other unnamed features (lat 32.8° S., long 268° E. and lat 36.5° S., long 267° E.) in the northeastern map area, display annuli of concentric fractures that characterize many coronae; these features are not included in the corona database of Stofan and others (1992) and are considered volcanic features (called patera). Parts of the annuli of these three tectonomagmatic features cut unit Pc, but materials of this unit also seem to embay the annuli of these tectonomagmatic features, suggesting synchronous development of unit Pc and formation of these three structures. In Nordenflycht Patera, young flows of unit fchP crosscut the annulus and fill its interior. Concentric fractures also postdate flows of unit fchP, indicating that annulus formation continued after emplacement of the youngest corona-related flows.

Radial Fracture Systems

Radial fracture suites extend hundreds to thousands of kilometers across the surface of Venus. These radial systems, characterized by fractures and graben that radiate from a tectonomagmatic center (for example, caldera, corona), likely mark the surface manifestation of mafic dike swarms (McKenzie and others, 1992; Grosfils and Head, 1994; Ernst and others, 1995), although they could also represent cross-sectional hourglass structures (Schultz and others, in press). In the map area, radial fracture systems are mostly centrally located in the transition between Parga Chasmata and Helen Planitia.

A north-south-oriented fracture system centered on Darclée Patera dominates eastern V–52. The fracture system is not uniformly arranged around an interpreted source. It contains a 350-km-long, densely fractured portion north of Darclée Patera and a less closely spaced fractured portion containing a fan morphology that extends more than 1,000 km to the south. Around Darclée Patera, volcanic flows cover the fractures. The absence of fractures east and west of the volcanic system could result from volcanic burial or from stress buttressing produced by basement units Pc and tu, located to the east and west, respectively. Stress butressing occurs in radial fracture systems on the Earth (for example, buttressing of the Spanish Peaks dike swarm by the Sangre de Cristo Mountain Range; Odé, 1957) and prevents dike propagation. The Darclée Patera system is defined by single lineaments interpreted as fractures, V–shaped fissures, and <2-km-wide, paired, dark and bright lineaments interpreted

as graben. Some fractures display en echelon offsets, which are patterns considered in terrestrial dike-related fracture systems to result from the rotation of the underlying dike segment at shallow depth due to changes in the stress field or changes in host rock rheology (Pollard, 1987). The presence of shields aligned along fractures in the southern part of the fracture system is consistent with subsurface dikes. Flows at fracture terminations or other indications of magma beneath the fractures, such as the existence of pit chains, are not observed.

If we consider the radial fracture systems to be underlain by dikes that propagate laterally through the host rock (McKenzie and others, 1992; Grosfils and Head, 1994, 1995, 1996; Ernst and others, 1995), local stress related to the existence of a pressurized magma body would control the radial pattern. As dikes propagate, regional stresses are more important than local magma-source-related stresses, and the plan-view geometry of radial dyke swarms adopts patterns controlled by regional principal stress directions (Ernst and others, 1995). Fracture systems adjacent to chasmata of the Beta-Atla-Themis volcanic zone trend generally parallel to the regional fracture directions, which is consistent with fracture systems aligned with the regional maximum horizontal compressive stress direction. The fracture system centered on Darclée Patera is oblique to the northwest-trending fracture belt, suggesting that the fracture system of Darclée Patera was emplaced before fracture belt formation. The trend of fractures south of Darclée Patera, where fractures reach the farthest from the source and are, therefore, most sensitive to local modifications of the regional stress field, is locally modified around the unnamed corona (lat 41.6° S., long 265.5° E.). Fractures of the Darclée Patera radial system cut most materials in the eastern map area, including units tu, pHu, fsU, and hu. Radial fractures of the Darclée Patera system and materials of unit fsU seem diachronous; fractures cut unit fsU, yet shields and associated materials of fsU appear genetically related to fractures of the radial fracture system. Younger volcanic materials (unit fmA) in the southeastern map area and corona-related materials related to Parga Chasmata (unit fchP) postdate radial fracture formation.

Two other radial fracture systems occur in the center of the map area: one centered on Monoshi Tholus and the other centered on an unnamed patera (lat 40.5° S., long 258° E.). These fracture systems are arranged around the volcanic centers and are only absent where they are buried by flows and shield clusters. East of Monoshi Tholus, graben evolved to fissures, possibly indicating a decrease in dike width and (or) depth (Pollard and others, 1983). The radial fracture system centered at lat 40.5° S., long 258° E. exhibits pit chains, which is evidence of subsurface magma flow. The sharp radial disposition of both of these systems indicates a major influence by the local stress field that is produced around the volcanic center and minor modification in the trend of the distal fractures to the northeast and northwest of Monoshi Tholus. Shield-related materials of unit sfMo bury and, hence, postdate the fracture system centered on Monoshi Tholus. Some of the shields seem to be related to the radial fractures, so shield emplacement might be locally controlled by the fracture system. Radial fractures of the system centered at lat 40.5° S., long 258° E. are associated with materials of unit fsU. The alignment of shields with radial pits and fractures is consistent with a genetic relation between the shields and fractures.

Localized Deformation

Different suites of parallel, kilometer-scale lineaments, interpreted as extension fractures on the basis of their narrow, linear geometry and their character relative to radar illumination (Banerdt and Sammis, 1992), cut different materials in the map area. The consistent spacing and trend imply that these fractures represent single, genetically related fracture sets. In the northeastern map area, superimposed suites of parallel, fine-scale lineaments cut the materials of unit Pc in a reticulate pattern composed of intersecting north and west-northwest fractures that are both formed by constant-spaced lineaments (<2 km) as long as ~100 km. The lineament trends change locally around volcanic structures. Similar reticulate patterns are preserved in unit fchP, in the interior of Hervor Corona, and in unit fpW near Witte Patera. In each location, Parga Chasmata and the corona-related structures postdate formation of the reticulate fracture suite.

Two models could explain these constant, regularly spaced fracture suites: (1) fracturing in a layer of constant thickness similar to fracture spacing, which is a situation observed in joints within terrestrial sedimentary layers (Pollard and Aydin, 1988) or (2) a shear-lag model that occurs in a layer of variable thickness partially decoupled from a similar underlying material by frictional contact (Banerdt and Sammis, 1992). It is impossible to constrain the thickness of the deformed layer to favor one of the models, but it seems unlikely that two areas that are separated by more that 2,000 km (units Pc, fpW) and are found in different geologic settings would display the same layer thickness; thus, the shear-lag model seems to be a more likely hypothesis.

In the southern map area, two orthogonal northeast- and northwest-trending graben cut unit pHu at lat 41.7° S., long 251° E. but are covered by shield related materials of unit hu, helping to constrain the time relation between the units. Orthogonal graben, spaced 7–30 km apart, display about 2-km widths.

Impact Features

The Helen Planitia quadrangle hosts eleven impact structures that range from 6 to 44 km in diameter (table 1); most are pristine impact structures that lack obvious volcanic embayment, despite the numerous volcanic features and associated units represented in the map area. Xenia, Viola, and Wollstonecraft represent multiple impact structures composed of two or more craters. In Xenia and Viola, small impact structures overlap the main crater, but a flooded doublet crater plus a smaller crater located on the ejecta form the multiple impact structure of Wollstonecraft. Doublet craters, formed by simultaneous impact of two separated projectiles, are likely the result of well-separated binary asteroids or atmospheric disruption of a single asteroid (Cook and others, 2003). Moore, Xenia, Kanik, Steinbach, and Wollstonecraft display radar-smooth interior floor materials, which could be related to crater formation but

more likely result from flooding long after crater formation (Izenberg and others, 1994; Herrick and Sharpton, 1999).

Local fracture suites cut the ejecta materials of two craters, Ustinya and Zerine. Ustinya, formed on unit pHu and partially embayed by shield-related materials of this same unit, is cut by local fracture sets. Zerine, located on unit fsZ, is cut by the radial fracture suite of Achall Corona.

Adaiah exhibits a parabolic halo of fine-grained material that forms a diffuse radar-rough layer to the west. This halo masks regional tectonic structures and the contact between units pHu and hu. Another radar-rough halo occurs in northwestern Helen Planitia quadrangle (V–52); four impact structures, Moore, Xenia, Kanik, and Rose, lie proximal to the halo, which partially mantles the contacts between units fcH, sfSi, and hu.

Three craterless splotches, interpreted as shock features formed by impactors that do not reach the surface (McKinnon and others, 1997), occur in the map area. Two features (lat 49.3° S., long 265.3° E. and lat 46.5° S., long 241.7° E.) display smooth interiors and rough borders. The third feature (lat 39° S., long 257.5° E.) marks a radar-rough splotch that lacks other features.

Surficial Deposits and Aeolian Marks

Evidence of wind-related processes and deposits are preserved in western Helen Planitia quadrangle (V–52). Wind streaks are formed by the interaction of local topography, sediment, and prevailing winds and allow the characterization of surface wind patterns (Greely and others, 1997). Two different morphologies occur in the map area: linear and volcano-related wind streaks. Radar-smooth, linear wind streaks (>200 km long) are observed in stretched images at lat 34° S., long 244° E. The wind streaks trend northeast, but wind vergence cannot be determined. Wind streaks associated with small volcanoes in the eastern map area formed as wind tails on the northeast flanks of the volcanoes and indicate a predominant northeast wind across the eastern map area. Guest and others (1992) propose that similar deposits in other volcanic plains represent ash-fall deposits and record evidence of limited pyroclastic activity.

Geologic History and Resurfacing Style

The surface of the Helen Planitia quadrangle (V–52) preserves a diverse assemblage of structures and materials, but the absence of distinctive temporal markers and robust impact-crater dating techniques (Hauck and others, 1998; Campbell, 1999) makes correlation of units across the map area difficult. Instead of a classical material description from older to younger, we follow geographic criteria describing relative time relations in the Parga Chasmata and Helen Planitia regions and subregions (western, central, and eastern). Within these regions and subregions, units that are in contact with and (or) interact with various structures or suites of structures allow the establishment of local temporal relations and, hence, a local history on the basis of reproducible observations.

Despite these mapping limitations, some general observations emerge about the evolution of the map area. Across Helen Planitia quadrangle, tessera terrain inliers and other basal materials (Parga Chasmata materials and Helen Planitia materals) form the substrate over which different volcanic units were emplaced. We cannot, however, determine the extent of tessera terrain and basal terrains beneath all units or the relative temporal evolution among various tessera terrain and basal terrain exposures. The various suites of secondary structures and deformation histories combined with the lack of contact relations between material units argues against a unique, coherent, synchronously formed basement layer for the entire quadrangle (for example, Basilevsky and Head, 1998).

The map area represents an area of transition between two topographic provinces, mesolands and lowlands, so the study of the resurfacing mechanisms is important to constrain whether changes in geologic style relate to this topographic transition. A varied assemblage of volcanic sources, including coronae, large volcanoes, rift-related fractures, medium-size edifices (volcanoes and steep-sided domes), and a large number of small shields contribute to resurfacing at scales from tens to thousands of kilometers across the map area. The regions adjacent to chasmata were resurfaced by extensive lava flows that originate from chasmata, coronae, and volcanic structures; individual flows extend more than 1,000 km from eruptive centers. Medium-size volcanoes and steep-sided domes scattered across the many corona-related units in the northern map area are diachronous relative to corona-related units. Local shield clusters associated with large tectonomagmatic features and individual groups of shields postdate the corona- and volcano-related flows. South of Parga Chasmata, resurfacing is dominated by volcano- and shield-related processes. Heterogeneous materials are a mixture of corona- and volcano-related flows, fields of dispersed volcanic edifices, and materials of undetermined origin. A lack of temporal constraints disallows interpretation of stratigraphic significance for this spatial change in resurfacing style.

Parga Chasmata Region

On the basis of crosscutting and local superposition relations, the earliest events recorded in the western PCR are the emplacement and subsequent tectonic deformation of basement materials: tessera terrain and local Parga Chasmata materials. The original characteristics of tessera terrain prior to the acquisition of deformation fabrics are unconstrained; although many workers assume that these materials had volcanic origins, evidence of emplacement mechanisms are obliterated by subsequent tectonism. The spatial and temporal distribution of these basement materials is similarly unconstrained; there is no evidence to indicate that (1) tessera terrain occurs at depth beneath all other materials or (2) that either the host material for tessera terrain or tessera terrain deformation predated the formation of the host materials of other basal materials. Tessera terrain displays an extensional ribbon fabric that indicates a shallow depth to the brittle-ductile transition (BDT) or a shallow depth to a sharp decrease in viscosity contrast at the specific time and specific location of ribbon formation (Hansen and Willis, 1998; Hansen, 2006). In the northwestern map area, flows and shield-related materials of volcanic basal units embay

ribbon-bearing tessera terrain preserved in local elevated areas. Heterogeneous materials, including flows and shield-related materials, then embay this assemblage of basement materials. Regional northwest-striking fractures cut the basement and heterogeneous materials and interact with local corona-related concentric fracture suites. Other regional deformation trends, such as northwest- and north-trending wrinkle ridges, also deform the heterogeneous materials. Corona-related materials of Parga Chasmata, locally emplaced over heterogeneous materials, embay regional and local fracture suites. Thus, northwestern Helen Planitia quadrangle records a sequence of events from basement terrain formation to corona-related materials related to Parga Chasmata. The formation of coronae and chasmata require the existence of a deep BDT (Hansen and others, 2000), so this sequence of materials also records a change in the local depth of the BDT from the shallow BDT conditions necessary to form ribbon-bearing tessera terrain to a deeper BDT condition necessary for Parga Chasmata formation. This relation requires a local change in the depth to BDT from shallow to deep wherever tessera terrain and coronae are spatially correlative and, therefore, across much of the map area, except central and eastern areas of the PCR where no tessera terrain units are exposed; although tessera terrain could occur at depth beneath the coronae and chasmata, the data do not require such a relation.

In the central map area, the basement material of Giltine Tesserae includes a set of individual inliers, including some that display ribbon-like structures and folds. The central and eastern areas of the PCR record formation and evolution of the regional extensional belt. The earliest events recorded in Parga Chasmata are emplacement and subsequent tectonic deformation of the Parga Chasmata materials. It is not clear if these materials are older terrains preserved inside the deformation belt or materials emplaced during the initial stages of chasmata formation. The different basal unit inliers, deformed by local suites of tectonic structures, are not in contact with one another; therefore, mutual temporal relations are unconstrained. Tessera terrain inliers and Parga Chasmata materials are postdated by flows originating from chasmata-related coronae and volcanic features, as well as from chasmata fractures. Corona-related flows and tectonic suites evolved in intimate spatial and temporal relation with the fracture belt, in an intertwined sequence of corona flows, local corona-related tectonic structures, and chasmata-related flows and structures that suggest coeval formation of coronae and Parga Chasmata. All the corona- and volcano-related flow units mapped in relation to Parga Chasmata are composite units comprised of diachronous flows as indicated by primary structures (for example, flow direction and flow fronts) and their relation to the fracture belt. After emplacement of corona-related materials, ribbon-like structures in Giltine Tesserae were reactivated, which probably related to the regional stress field responsible for Parga Chasmata; reactivated structures cut the corona-related materials.

Although volcano- and shield-related units bury extensive corona-related flows in the PCR, the composite nature of corona flows disallows extrapolation of locally established relative temporal relations between volcano-, shield-, and corona-related units across the map area. North-trending wrinkle ridges deform corona- and volcano-related flows. Temporal relations between the wrinkle ridges and chasmata fractures cannot be established. Point-sourced, shield-related volcanic deposits and medium-size volcanoes overlay all units. Shields are especially pervasive in the interior of large tectonomagmatic features and volcanoes, but they also occur in isolation or in small groups across the entire PCR.

Helen Planitia Region

Emplacement and subsequent tectonic deformation of tessera terrain in Sopdet Tesseare and Tsovinar Dorsa are the oldest events recorded in the western and central areas of the HPR. This tessera terrain exhibits a northwest-trending, pervasively developed tectonic fabric that may indicate a thin brittle layer in the area at the time of deformation. As with other tessera terrain, the original spatial distribution of this terrain is unconstrained. Basal Helen Planitia materials and shield-related materials locally bury the tessera terrain, as illustrated by embayment relations preserved along broad topographic warps in southwestern Helen Planitia quadrangle (for example, Tsovinar Dorsa). Basal materials are deformed by northwest-trending folds along the northwest-trending topographic rises of Sopdet Tesserae and Tsovinar Dorsa. Presumably folding/warping occurred prior to the emplacement of the embayment materials—heterogeneous materials that occupy most of the western HPR. These materials host thousands of shields across most of the map area; shields are distributed across the unit and developed at the edges of and within the basal materials. Locally, the shields coalesce to form a discontinuous layer that covers the older materials in a patchwork style, or shield paint (Hansen, 2005), that locally buries or reveals substrate material. Northwest-trending wrinkle ridges of the Helen Planitia trend (Billoti and Suppe, 1999) deform the heterogeneous materials; north-striking fractures and fracture belts cut both the heterogeneous materials and the wrinkle ridges. Shields locally cover and postdate wrinkle ridges and fractures, yet the shields are also locally cut by, or interact with, regional structures, suggesting diachronous temporal relations between the shields and the formation and (or) reactivation of structures. In the western HPR, coronae correlate spatially with north-striking fractures and fracture belts. Unlike the coronae related to Parga Chasmata, these coronae lack evidence for large associated flow units.

In the central and eastern area of the HPR, tessera terrain inliers in Norna and Ustrecha Tesserae represent the oldest local surface materials. The presence of short-wavelength ribbon fractures and orthogonal longer-wavelength folds in Norna Tesserae may indicate a deepening of the BDT or depth to a sharp decrease in viscosity during tessera formation. Other tessera terrain inliers are cut by local tectonic structures, although in all inliers the youngest deformation is marked by a suite of graben that are embayed by younger volcanic materials. The individual tessera terrain inliers are not in mutual contact; therefore, temporal relations are impossible to constrain. Together with tessera terrain, dispersed kipukas of Helen Planitia materials form the basement, which is overlain by a heterogeneous materials unit and shield and associated flows units. Temporally both units are time-transgressive, and both are deformed by wrinkle ridges

of the regional circum-Themis trend (Billoti and Suppe, 1999) and by north-striking regional fractures. Shields on these units postdate wrinkle ridges and fractures, yet they are also affected by these regional structures, suggesting that shield emplacement and regional deformation (or local structural reactivation) were diachronous.

Numerous coronae and large volcanoes are spatially associated with regional, north-striking fractures and fracture belts (for example, Ajina Fossae). As in the western HPR, these coronae lack obvious associated flow units. The absence of obvious flows could indicate a lack of an effusive stage, similarity of backscatter between possible flows and adjacent material, or surface backscatter homogenization caused by slow but time-persistent weathering (Arvidson and others, 1992). If homogenization is a function of time, slow weathering could suggest two temporally distinct coronae populations in the map area: older coronae related to north-striking fractures in the HPR and younger coronae located near or associated with Parga Chasmata. The general character of HPR coronae and PCR coronae are similar to old and young coronae of Chapman and Zimbelman (1998), respectively.

Locally younger materials in the HPR are volcano-related units, formed in relationship with north-trending fracture belts, shield clusters, and associated materials in corona interiors.

Interaction between materials of HPR and PCR occurs in the central map area. In this transition zone, corona- and volcano-related flows locally postdate basement and heterogeneous materials in both regions. Individual shields postdate these units, suggesting that shield-related, point-distributed volcanic activity was also diachronous during emplacement of these units.

In summary, geologic mapping reveals a range of resurfacing mechanisms (extensive volcano- and corona-related flows and regional resurfacing by shield-related coalesced material) and a geographic transition in the predominant resurfacing style from corona- and volcano-dominated large flows associated with Parga Chasmata to a patchy discontinuous shield terrain that characterizes much of southern Helen Planitia quadrangle (V–52). Coronae-, volcano-, and shield-related volcanic activity occurred across the map area and apparently was not restricted to a particular material or time. Similarly, local and regional tectonic suites that affect the different materials in the map area were not restricted to a particular material or time. The results of geologic mapping are inconsistent with global stratigraphic models (Basilevsky and Head, 1998), which call for synchronous development of the same units across globally extensive regions. In contrast, geologic relations within the Helen Planitia quadrangle record local complex histories that vary both spatially and temporally (for example, Phillips and Hansen, 1998; Guest and Stofan, 1999).

References Cited

Addington, E.A., 2001, A stratigraphic study of small volcano clusters on Venus: Icarus, v. 149, p. 16–36.

Arvidson, R.E., Greely, R., Malin, M.C., and 5 others, 1992, Surface modification of Venus as inferred from Magellan observations of plains: Journal of Geophysical Research, v. 97, p. 13,303–13,318.

Baker, V.R., Komatsu, G., Gulick, V.C., and Parker, T.J., 1997, Channels and valleys, *in* Bouger, S.W., Hunten, D.M., and Phillips, R.J., eds., Venus II—Geology, geophysics, atmosphere, and solar environment: Tuscon, The University of Arizona Press, p. 757–793.

Baker, V.R., Komatsu, G., Parker, T.J., and 3 others, 1992, Channels and valleys on Venus—Preliminary analysis of Magellan data: Journal of Geophysical Research, v. 97, p. 13,421–13,444.

Banerdt, W.B., McGill, G.E., and Zuber, M.T., 1997, Plains tectonism on Venus, *in* Bouger, S.W., Hunten, D.M., and Phillips, R.J., eds., Venus II—Geology, geophysics, atmosphere, and solar environment: Tuscon, The University of Arizona Press, p. 901–930.

Banerdt, W.B., and Sammis, C.G., 1992, Small-scale fracture patterns on the volcanic plains of Venus: Journal of Geophysical Research, v. 97, p. 16,149–16,166.

Basilevsky, A.T., and Head, J.W., 1995, Regional and global stratigraphy of Venus—A preliminary assessment and implications for the geologic history of Venus: Planetary and Space Science, v. 43, p. 1523–1553.

Basilevsky, A.T., and Head, J.W., 1998, The geologic history of Venus—A stratigraphic view: Journal of Geophysical Research, v. 103, p. 8531–8544.

Basilevsky, A.T., and Head, J.W., 2000, Geologic units on Venus—Evidence for their global correlation: Planetary and Space Science, v. 48, p. 75–111.

Basilevsky, A.T., and Head, J.W., 2004, Airfall crater deposits on the surface of Venus—Do we see them in the Venera panoramas? [abs.], *in* 35th Lunar and Planetary Science Conference: Houston, Tex., Lunar and Planetary Institute, Abstract #1133 [CD-ROM].

Basilevsky, A.T., Head, J.W., Schaber, G.G., and Strom, R.G., 1997, The resurfacing history of Venus, *in* Bouger, S.W., Hunten, D.M., and Phillips, R.J., eds., Venus II—Geology, geophysics, atmosphere, and solar environment: Tucson, The University of Arizona Press, p. 1047–1084.

Billoti, F., and Suppe, J., 1999, The global distribution of wrinkle ridges on Venus: Icarus, v. 139, no. 1, p. 137–159.

Bleamaster, L.F., and Hansen, V.L., 2001, The Kuanja/Vir-Ava Chasmata—A coherent intrusive complex on Venus [abs.], *in* Lunar and Planetary Science Conference XXXII: Houston, Tex., Lunar and Planetary Institute, Abstract #1316 [CD-ROM].

Brown, C.D., and Grimm, R.E., 1997, Tessera deformation and the contemporaneous thermal state of the plateau highlands, Venus: Earth and Planetary Science Letters, v. 147, p. 1–10.

Bullock, M.A., and Grinspoon, D.H., 2001, The Recent Evolution of Climate on Venus: Icarus, v. 150, p. 19–37.

Butler, B.C.M., and Bell, J.D., 1988, Interpretation of Geological Maps: New York, John Wiley & Sons, 236 pp.

Byrnes, J.M., 2002, Lava flow field emplacement studies of Mauna Ulu (Kilauea volcano, Hawaii, USA) and Venus using field and remote sensing analyses: Pittsburgh, Penn.,

University of Pittsburgh, Ph.D. dissertation.
Campbell, B.A., 1999, Surface formation rates and impact crater densities on Venus: Journal of Geophysical Research, v. 104, p. 21,951–21,955.
Chapman, M.G., 1999, Geologic map of the Galindo quadrangle (V–40), Venus: U.S. Geological Survey Geologic Investigations Series I–2613, scale 1:5,000,000 [http://geopubs.wr.usgs.gov/i-map/i2613/].
Chapman, M.G., and Zimbelman, J.R., 1998, Corona associations and their implications for Venus: Icarus, v. 132, no. 2, p. 344–361.
Compton, R.R., 1985, Geology in the field: New York, John Wiley & Sons, 398 pp.
Cook, C.M., Melosh H.J., and Bottke, W.F., Jr., 2003, Doublet craters on Venus: Icarus, v. 165, p. 90–100.
Crisp, D., and Titov, D., 1997, The thermal balance of the Venus atmosphere, *in* Bougher, S.W., Hunten, D.M., and Phillips, R.J., eds., Venus II—Geology, geophysics, atmosphere, and solar wind environment: Tucson, The University of Arizona Press, p. 353–384.
Crumpler L.S., Aubele, J.C., Senske, D.A., and 3 others, 1997, Volcanoes and centers of volcanism on Venus, *in* Bouger, S.W., Hunten, D.M., and Phillips, R.J., eds., Venus II—Geology, geophysics, atmosphere, and solar wind environment: Tucson, The University of Arizona Press, p. 697–756.
Crumpler, L.S., Head J.W., and Aubele, J.C., 1993, Relation of major volcanic center concentration on Venus to global tectonic patterns: Science, v. 261, p. 591–595.
Daily, M., and Stewart, H.E., 1979, Lineament mapping with orbiting imaging radar: American Association of Petroleum Geologists Bulletin, v. 63, no. 3, p. 825.
DeShon, H.R., Young, D.A., and Hansen, V.L., 2000, Geologic evolution of southern Rusalka Planitia, Venus: Journal of Geophysical Research, v. 105, p. 6983–6995.
Donahue, T.M., Grinspoon, D.H., Hartle, R.E., and Hodges, R.R., 1997, Ion/neutral escape of hydrogen and deuterium—Evolution of water, *in* Bougher, S.W., Hunten, D.M., and Phillips, R.J., eds., Venus II—Geology, geophysics, atmosphere, and solar wind environment: Tucson, The University of Arizona Press, p. 385–414.
Ernst, R.E., Head, J.W., Parfitt, E., Grosfils, E., and Wilson, L., 1995, Giant radiating dyke swarms on Earth and Venus: Earth Science Reviews, v. 39, p. 1–58.
Ferrill, D.A., Wyrick, D.Y., Morris, A.P., Sims, D.W., and Franklin, N.M., 2004, Dilational fault slip and pit chain formation on Mars: GSA Today, v. 14, p. 4–12.
Ford, J.P., Blom, R.G., Crisp, J.A., and 6 others, 1989, Spaceborne radar observations—A guide for Magellan radar-image analysis: Pasadena, Calif., Jet Propulsion Laboratory Publication 89–41, 126 p.
Ford, J.P., Plaut, J.J., Weitz, C.M., and 5 others, 1993, Guide to Magellan image interpretation: Pasadena, Calif., National Aeronautics and Space Administration, Jet Propulsion Laboratory Publication 93-24, 287 pp.
Ghent, R.R., and Hansen, V.L., 1999, Structural and kinematic analysis of Eastern Ovda Regio, Venus—Implications for crustal plateau formation: Icarus, v. 139, p. 116–139.
Gilbert, G.K., 1886, Inculcation of the scientific method: American Journal of Science, v. 31, p. 284–299.
Gilmore, M.S., Collins, G.C., Ivanov, M.A., Marinangeli, L., and Head, J.W., 1998, Style and sequence of extensional structures in tessera terrain, Venus: Journal of Geophysical Research, v. 103, p. 16,813–16,840.
Greely, R., Ardvison, R.E., Elachi, C., and 8 others, 1992, Aeolian features on Venus: Journal of Geophysical Research, Preliminary Magellan results, v. 97, p. 13,319–13,345.
Greely R., Bender, K.C., Saunders, R.S., Schubert, G., and Weitz, C.M., 1997, Aeolian processes and features on Venus, *in* Bougher, S.W., Hunten, D.M., and Phillips, R.J., eds., Venus II—Geology, geophysics, atmosphere, and solar environment: Tucson, The University of Arizona Press, p. 547–589.
Grosfils, E.B., and Head, J.W., 1994, Emplacement of radiating dike swarms in western Vinmara Planitia, Venus—Interpretation of the regional stress field orientation and subsurface magmatic configuration: Earth, Moon, and Planets, v. 66, p. 153–171.
Grosfils, E.B., and Head, J.W., 1995, Radiating dike swarms on Venus—Evidence for the emplacement at zones of neutral buoyancy: Planetary and Space Science, v. 43, p. 1555–1560.
Grosfils, E.B., and Head, J.W., 1996, The timing of giant radiating dike swarm emplacement on Venus—Implications for resurfacing of the planet and its subsequent evolution: Journal of Geophysical Research, v. 101, p. 4645–4656.
Guest, J.E., Bulmer, M.H., Aubele, J.C., and 6 others, 1992, Small volcanic edifices and volcanism in the plains of Venus: Journal of Geophysical Research, v. 97, p. 15,949–15,966.
Guest, J.E., and Stofan, E.R., 1999, A new view of the stratigraphic history of Venus: Icarus, v. 139, p. 55–66.
Hansen, V.L., 2000, Geologic mapping of tectonic planets: Earth and Planetary Science Letters, v. 176, p. 527–542.
Hansen, V.L., 2005, Venus's shield terrain: Geological Society of America Bulletin, v. 117, no. 5/6, p. 808–822.
Hansen, V.L., 2006, Geologic constraints on crustal plateau surface histories, Venus—The lava pond and bolide impact hypotheses: Journal of Geophysical Research, v. 111 (doi:10.1029/2006JE002714).
Hansen, V.L., Banks, B.K., and Ghent, R.R., 1999, Tessera terrain and crustal plateaus, Venus: Geology, v. 27, p. 1071–1074.
Hansen, V.L., Phillips, R.J., Willis, J.J., and Ghent, R.R., 2000, Structures in tessera terrain, Venus—Issues and answers: Journal of Geophysical Research, v. 105, p. 4135–4152.
Hansen, V.L., and Willis, J.J., 1996, Structural analysis of a sampling of tesserae—Implications for Venus geodynamics: Icarus, v. 123, no. 2, p. 296–312.
Hansen, V.L., and Willis, J.J., 1998, Ribbon terrain formation, southwestern Fortuna Tessera, Venus—Implications for lithosphere evolution: Icarus, v. 132, p. 321–343.
Hauck, S.A., Phillips, R.J., and Price, M.H., 1998, Venus—Crater distribution and plain resurfacing models: Journal of Geophysical Research, 103, p. 13,635–13,642.
Herrick, R.R., and Sharpton, V.L., 1999, There are a lot more

embayed craters on Venus than previously thought, *in* Lunar and Planetary Science Conference XXX: Houston, Tex., Lunar and Planetary Institute, Abstract #1696 [CD-ROM].

Ivanov, M.A., and Head, J.W., 2001, Geologic map of the Lavinia Planitia Quadrangle (V–55), Venus: U.S. Geological Survey Geologic Investigation Series I–2684, scale 1:5,000,000 [http://pubs.usgs.gov/imap/i2684/].

Izenberg, N.R., Arvidson, R.E., and Phillips, R.J., 1994, Impact crater degradation on Venusian plains: Geophysical Research Letters, v. 21, p. 289–292.

Janes D.M., Squyres, S.W., Bindschadler, D.L., and 4 others, 1992, Geophysical models for the formation and evolution of coronae on Venus: Journal of Geophysical Research, v. 97, p. 16,055–16,067.

Johnson, J.R., Komatsu, G., and Baker, V.R., 1999, Geological map of the Barrymore quadrangle (V–59), Venus: U.S. Geological Survey Geologic Investigations Series Map I–2610, scale 1:5,000,000 [http://geopubs.wr.usgs.gov/i-map/i2610].

Kirk, R.L., Soderblom, L.A., and Lee, E.L., 1992, Enhanced visualization for interpretation of Magellan radar data—Supplement to the Magellan special issue: Journal of Geophysical Research, v. 97, p. 16,371–16,381.

Koch, D.M., and Manga, M., 1996, Neutrally buoyant diapirs—A model for Venusian coronae: Geophysical Research Letters, v. 102. p. 225–228.

Mackwell, S.J., Zimmerman, M.E., and Kohlstedt, D.L., 1998, High-temperature deformation of dry diabase with application to tectonics on Venus: Jounal of Geophysical Research, v. 103, p. 975–984.

Maltman, A., 1990, Geological Maps—An Introduction: New York, Van Nostrand Reinhold, 184 pp.

McGill, G.E., and Campbell, B.A., 2004, Ages of Venusian ridge belts relative to regional plains [abs.], *in* Lunar and Planetary Science Conference XXXV: Houston, Tex., Lunar and Planetary Institute, Abstract #1143 [CD-ROM].

McKenzie, D., McKenzie, J.M., Saunders, R.S., 1992, Dike emplacement on Venus and on Earth: Journal of Geophysical Research, v. 97, p. 15,977–15,990.

McKinnon, W.B., Zahnle, K.J., Ivanov, B.A., and Melosh, H.J., 1997, Cratering on Venus—Models and observations, *in* Bouger, S.W., Hunten, D.M., and Phillips, R.J., eds., Venus II— Geology, geophysics, atmosphere, and solar environment: Tucson, The University of Arizona Press, p. 931–965.

Odé, H., 1957, Mechanical analysis of the dike pattern of the Spanish Peaks area, Colorado: Geological Society of America Bulletin, v. 68, p. 567–576.

Okubo, C.H., and Martel, S.J., 1998, Pit crater formation on Kilauea volcano, Hawaii: Journal of Volcanology and Geothermal Research, v, 86, p. 1–18.

Phillips, R.J., Bullock, M.A., Hauck, S.A., II, 2001, Climate and interior coupled evolution on Venus: Geophysical Research Letters, v. 28, p. 1779–1782.

Phillips, R.J., and Hansen, V.L., 1998, Geological evolution of Venus—Rises, plains, plumes and plateaus: Science, v. 279, p. 1492–1497.

Pollard, D.D., 1987, Elementary fracture mechanics applied to the structural interpretation of dykes, *in* Halls, H.C., and Fahrig, W.F., eds., Mafic dyke swarms: Geological Association of Canada Special Paper 34, p. 5–24.

Pollard, D.D., and Aydin, A., 1988, Progress in understanding jointing over the last century: Geological Society of America Bulletin, v. 100, p. 1181–1204.

Pollard, D.D., Delaney, P.T., Duffield, W.A., Endo, E.T., and Okamura, A.T., 1983, Surface deformation in volcanic rift zones: Tectonophysics, v. 94, p. 541–584.

Price, N., and Cosgrove, J., 1990, Analysis of Geological Structures: New York, Cambridge University Press, 502 p.

Ramberg, H., 1955, Natural and experimental boudinage and pinch-and-swell structures: Journal of Geology, v. 63, p. 512–526.

Sandwell, D.T., Johnson, C.L., Billoti, F., and Suppe, J., 1997, Driving forces for limited tectonics on Venus: Icarus, v. 129, p. 232–244.

Schultz, P., 1992, Atmospheric effects on ejecta emplacement and crater formation on Venus from Magellan: Journal of Geophysical Research, v. 97, p. 16,183–16,248.

Schultz, R.A., Moore, J.M, Grosfils, E.B., Tanaka, K.L., and Mège, D., in press, The Canyonlands model for "simple" planetary grabens—Revised physical basis and implications, in Chapman, M.G., and Skilling, I.P., eds., The geology of Mars—Evidence from Earth-based analogues: Cambridge University Press.

Schultz, R.A., Okubo, C.H., Goudy, C.L., and Wilkins, S.J., 2004, Igneous dikes on Mars revealed by Mars Orbiter Laser Altimeter topography: Geology, v. 32, p. 889–892.

Skinner, J.A., Jr., and Tanaka, K.L., 2003, How should planetary map units be defined? [abs.], *in* Lunar and Planetary Science Conference XXXIV: Houston, Tex., Lunar and Planetary Science Institute, Abstract #2100, [CD-ROM].

Squyres, S.W., Janes, D.M., Baer, G., and 4 others, 1992, The morphology and evolution of coronae on Venus: Journal of Geophysical Research, v. 97, p. 13,611–13,634.

Stofan, E.R., Hamilton, V.E., Janes, D.M., and Smrekar, S.E., 1997, Coronae on Venus—Morphology and origin, *in* Bouger, S.W., Hunten, D.M., and Phillips, R.J., eds., Venus II—Geology, geophysics, atmosphere, and solar environment: Tucson, The University of Arizona Press, p. 931–965.

Stofan, E.R., Sharpton, V.L., Schubert, G., and 4 others, 1992, Global distribution and characteristics of coronae and related features on Venus—Implications for origin and relation to mantle processes: Journal of Geophysical Research, v. 97, p. 13,347–13,378.

Stofan, E.R., Smrekar, S.E., and Martin, P., 2000, Coronae of Parga Chasma, Venus—Implications for chasma and corona evolution, in Lunar and Planetary Science Conference XXXI: Houston, Tex., Lunar and Planetary Institute, Abstract #1578 [CD-ROM].

Talbot, C.J., 1970, The minimum strain ellipsoid using deformed quartz veins: Tectonophysics, v. 9, p. 47–76.

Tanaka, K.L., Moore, H.J., Schaber, G.G., and 9 others, 1994, The Venus geologic mappers' handbook: U.S. Geological Survey Open-File Report 94–438.

Wilhelms, D.E., 1990, Geologic mapping, *in* Greeley, R., and Batson, R.M., eds., Planetary Mapping: New York, Cambridge University Press, p. 208–260.

Young, D.A., and Hansen, V.L., 2003, Geologic map of the Rusalka quadrangle (V–25), Venus: U.S. Geological Survey Geologic Investigations Series, I–2783, scale 1:5,000,000 [http://pubs.usgs.gov/imap/i2783/].

Zimbelman, J.R., 2001, Image resolution and evaluation of genetic hypotheses for planetary landscapes: Geomorphology, v. 37, p. 179–199.

Table 1. *Crater data for the Helen Planitia quadrangle (V–52), Venus. Y, yes; N, no*

Crater	Latitude (°S.)	Longitude (°E.)	Diameter (km)	Underlying unit/units	Ejecta blanket	Impact halo	Central peak	Rim	Interior flooding	Modification	Other Characteristics
Moore	30.35	248.40	21.1	hu	Y	Y	Y	Y	Y	Pristine	
Xenia	30.35	249.42	13.5	hu	Y	Y	N	Y	Y?	Pristine	Doublet crater
Kanik	32.54	249.87	16.5	hu, fc0A	Y	Y	Y	Y	Y	Pristine	
Viola	36.11	240.51	10	fcH	Y	N	N	Y	N	Pristine	Doublet crater
Rose	35.16	248.22	15.5	tu, sfSi, ftA	Y	N	N	Y	N	Pristine	
Zerine	29.57	258.60	6.5	fsZ, fc0A	Y	N	N	Y	N	Fractured	
Adaiah	47.28	253.35	18	hu	Y	Y	Y	Y	N?	Y	
Ustinya	41.16	251.64	11.8	pHu	Y	N	N	Y	N	Y	
Steinbach	41.42	256.94	20.3	hu	Y	N	Y	Y	Y	Y	
Shasenem	44.05	258.92	9	hu	Y	N	N	Y	N	Y	
Wollstonecraft	39.14	260.81	44.1	hu, fsU	Y	N	Y?	Y	Y	Y	Triplet crater